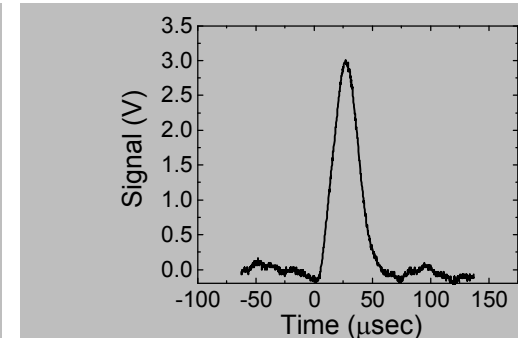
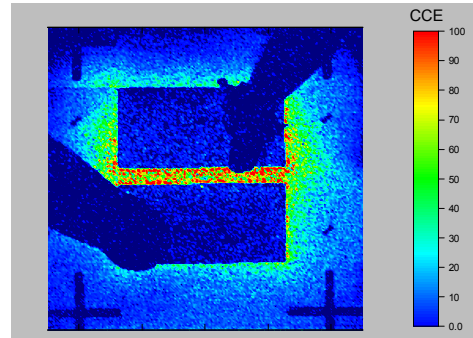


Exceptional service in the national interest



Single ion detection in diamond: A path for deterministic color center creation



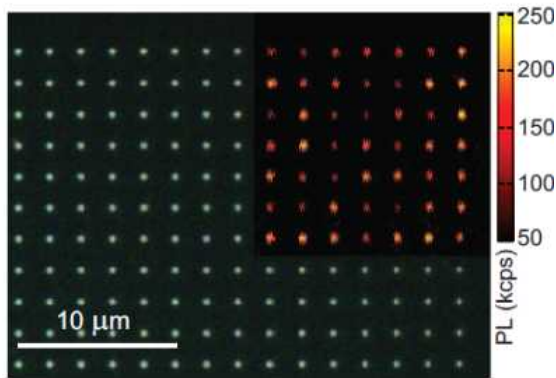
J. Abraham, B. Aguirre, J. Pacheco,
G. Vizkelethy, E. Bielejec

Deterministic Fabrication

Spatial localization **Established** → Masking - NV S. Sangtawesin et. al. Appl. Phys. Lett. 105, 063107 (2014)

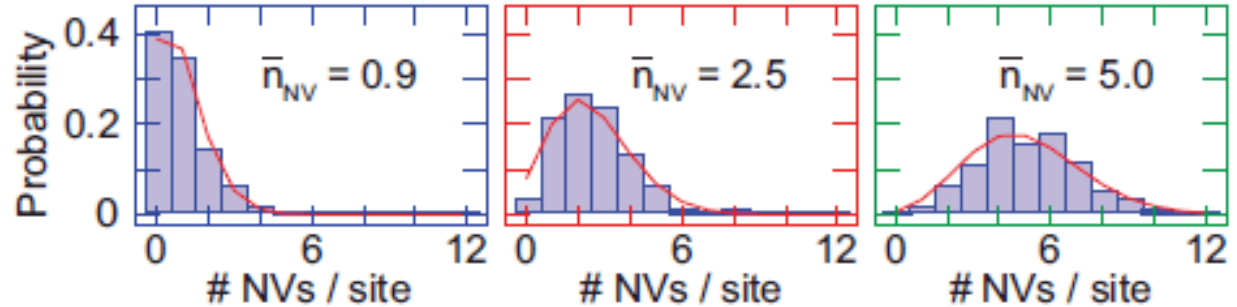
Yield **In progress** → Focused Ion Beam - SiV S. Tamura et. al. Appl. Phys. Express 7, 115201 (2014)
 SNL - nanImplanter

S. Sangtawesin et. Al. Appl. Phys. Lett. 105, 063107 (2014)

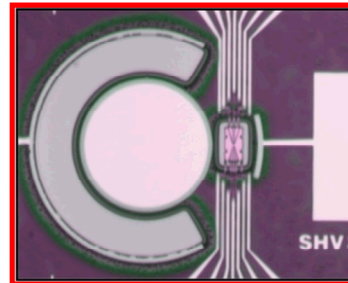


Poisson Statistics

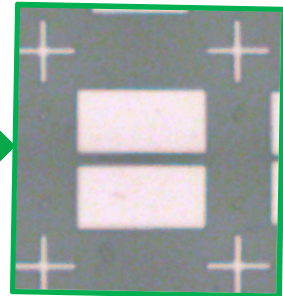
(Uncertainty in number of centers)



Single Ion Detector in Silicon



Single Ion Detector in Diamond



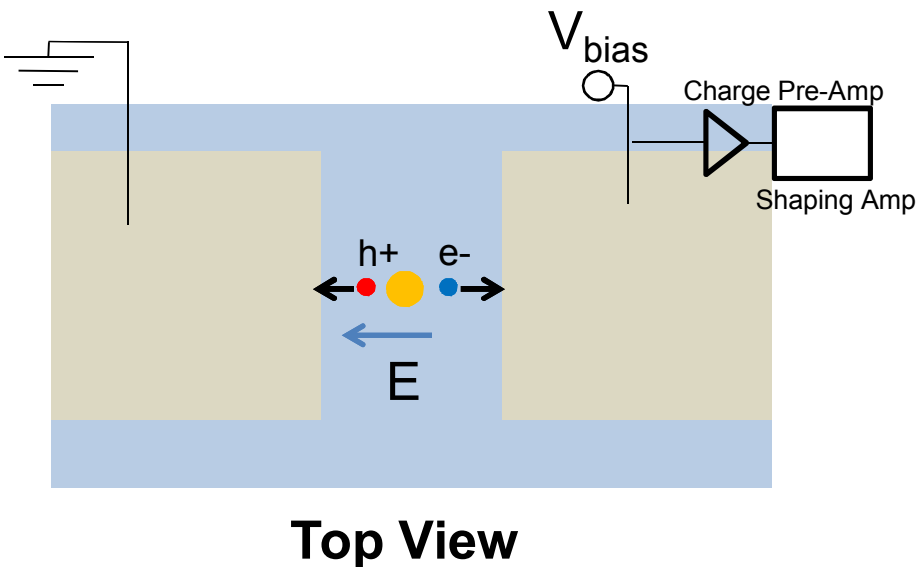
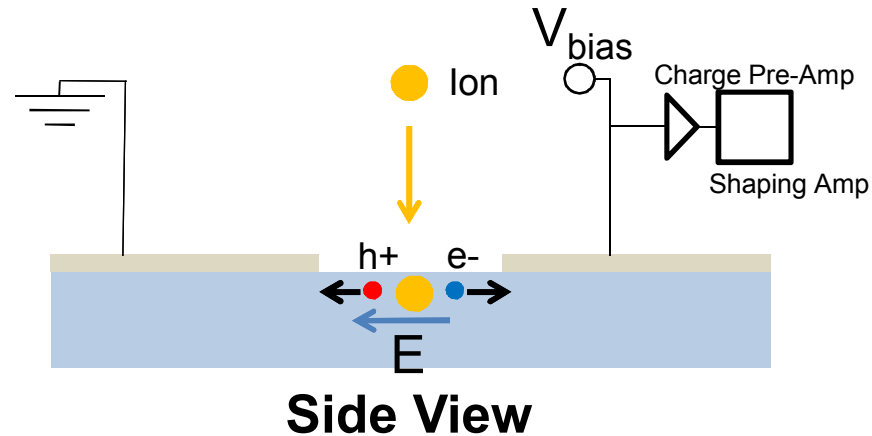
Our work:
 Translating single ion detection to diamond

J.A. Seamons, et. al. Appl. Phys. Lett, 93, 043124 (2008)
 E Bielejec, et. al. Nanotechnology 21, 085201 (2010)

In-situ single ion detection is a demonstrated path for yield control

By counting in ions, we will remove a source of Poisson statistics

Physics of Ion Detection



Shockley-Ramo Theorem:

$$i = q\vec{v} \cdot \vec{E}$$

Moving charges in an electrical field will induce a current on the electrodes applying the bias

Charge Collection Efficiency (CCE):

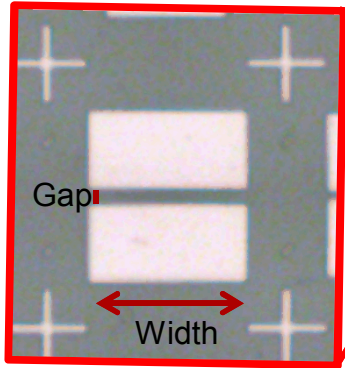
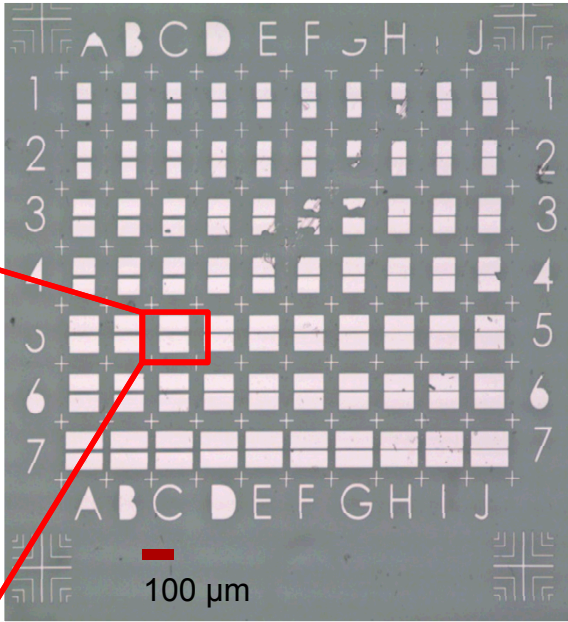
$$CCE = \frac{\text{Charge Collected}}{\text{Charge Deposited}} \times 100$$

Ion Beam Induced Charge (IBIC):

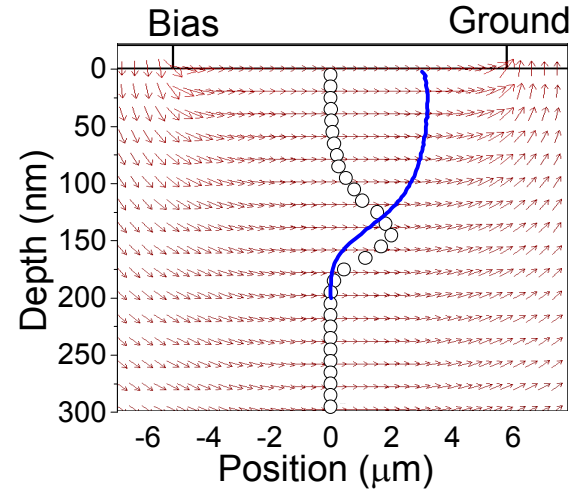
Ion Beam is rastered across device to measure the Charge Collection Efficiency (CCE) as a function of position

Fabrication/Modeling

Co-planar
Surface
Electrode
Detector

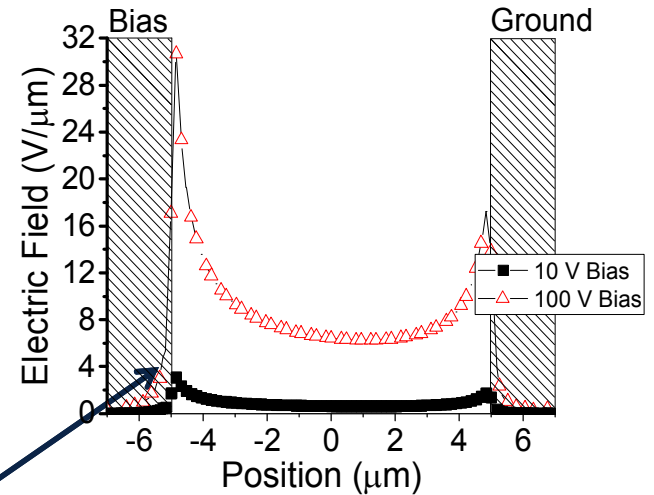


TCAD/SRIM simulation



Fabrication

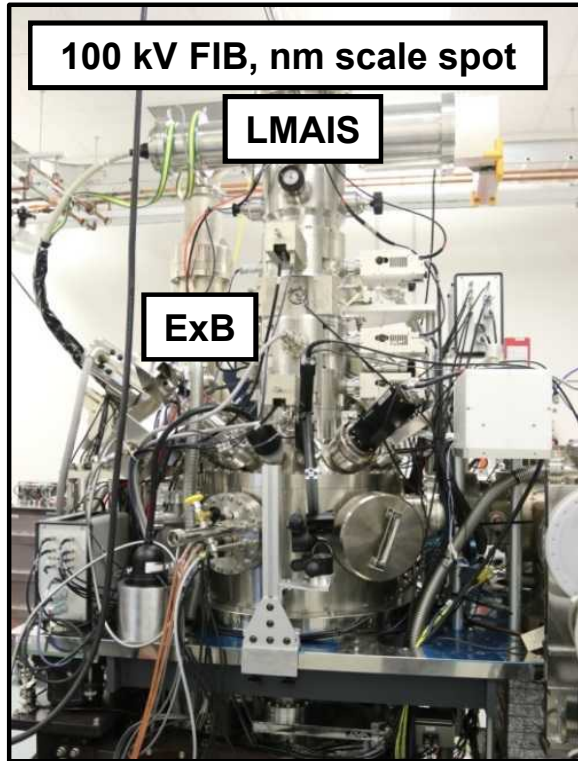
- Electronic grade single crystal diamond (Element 6)
- 200 nm Ti/Pt/Au Electrodes
- Varied width and gap spacing
 - 50-125 μm width
 - 2 – 10 μm gaps



95% CCE
From E6

Detector Characterization

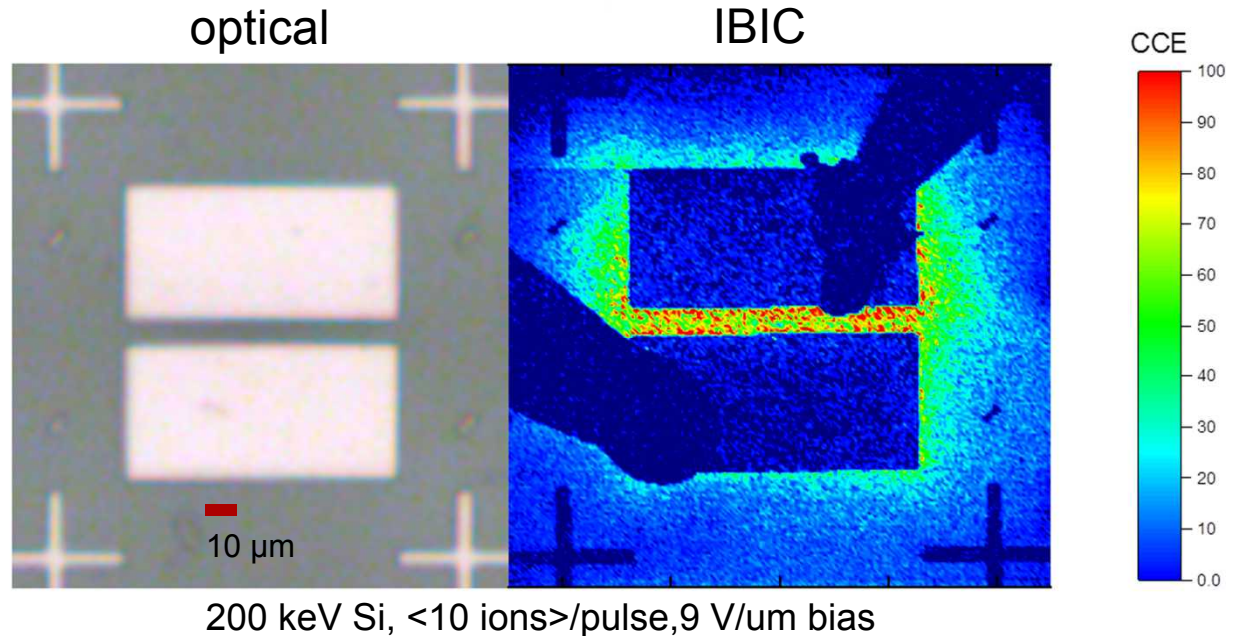
SNL Nanoimplanter (nl)



- Direct write lithography platform
→ nm targeting accuracy

Ion Beam Induced Current (IBIC)

$$\text{CCE} = \frac{\text{Charge Collected}}{\text{Charge Deposited}} \times 100$$



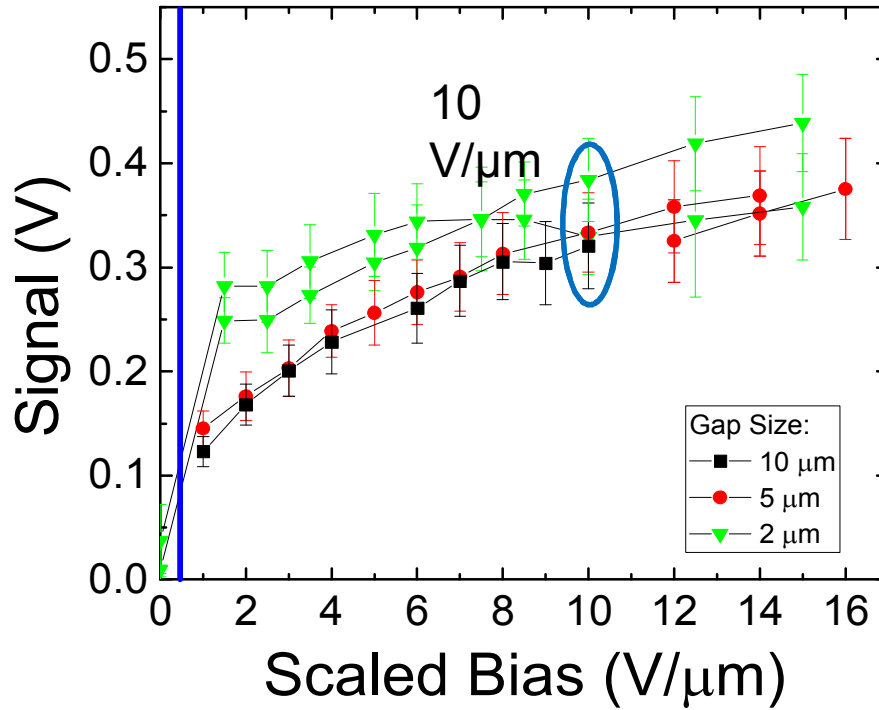
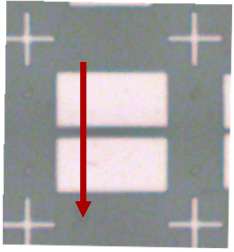
- Approaching 100% detection in the fielded gap

IBIC/Detection Demonstrated for low energy heavy ions

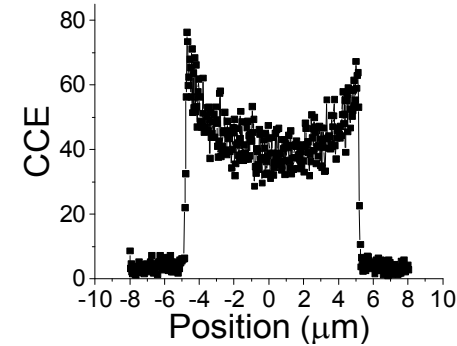
Detector Operation I

$\langle 100 \rangle$ ions/pulse = 100 +/- 10 ions/pulse

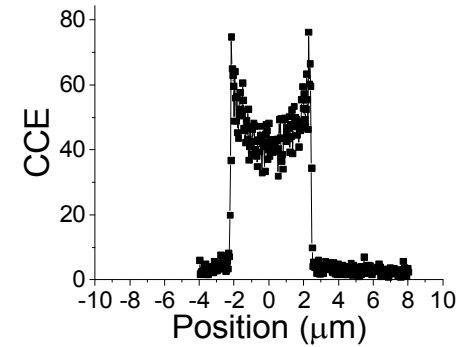
Y line cuts



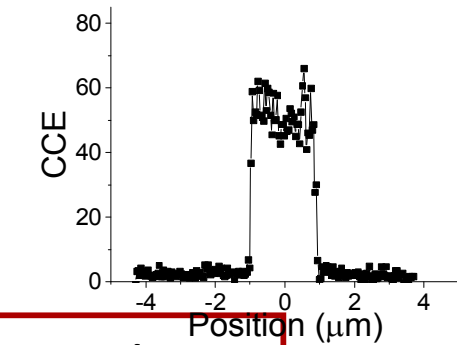
10 μm



5 μm



2 μm

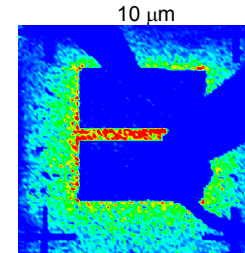
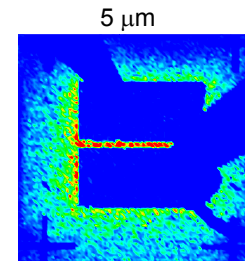
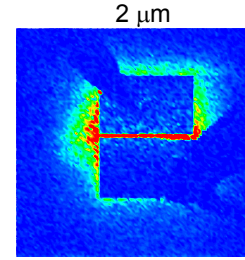
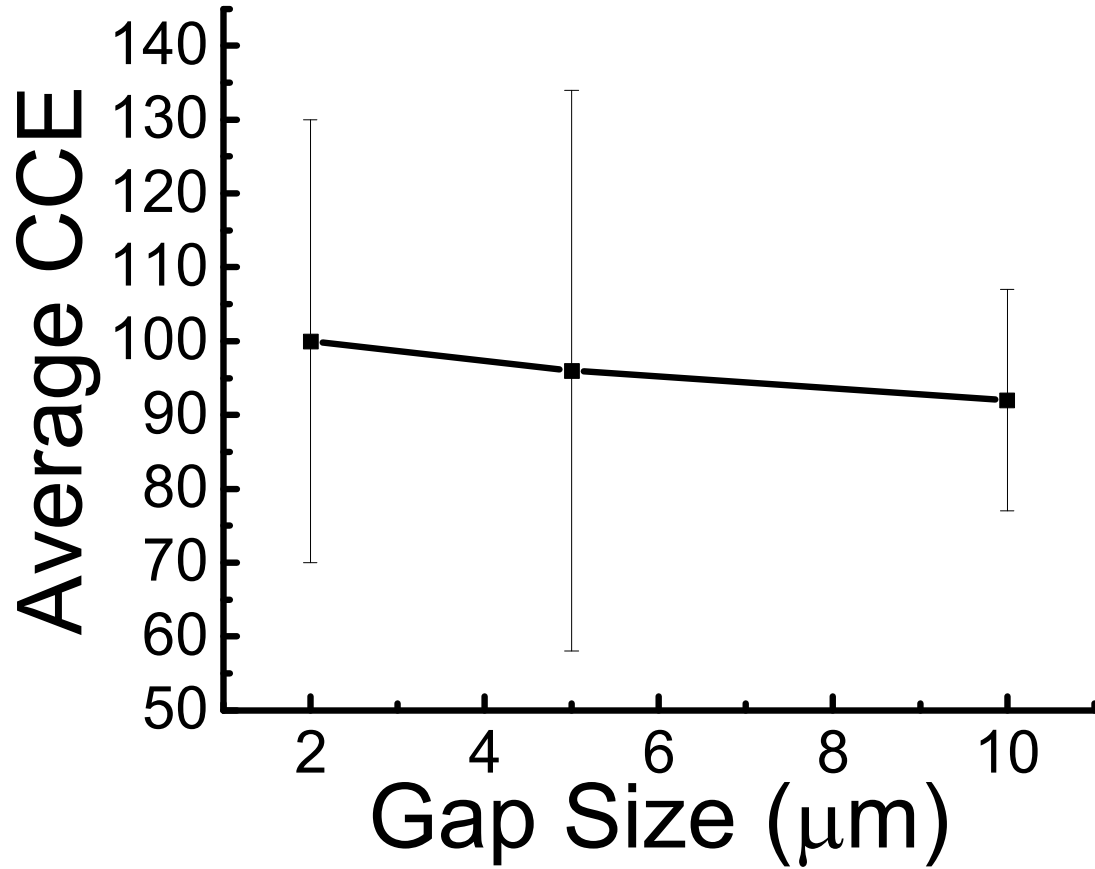


10^3 V/μm: Breakdown

Smaller Gap has a more uniform response and requires less bias for saturation

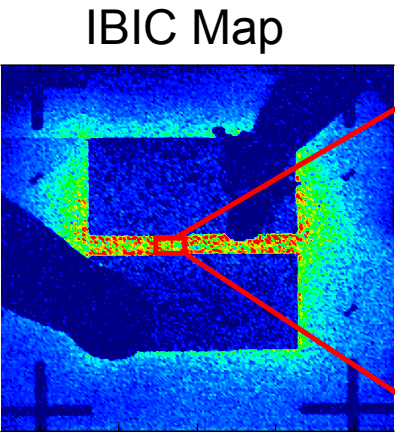
Detector Operation II

$\langle 10 \rangle$ ions/pulse = 10 +/- 3 ions/pulse

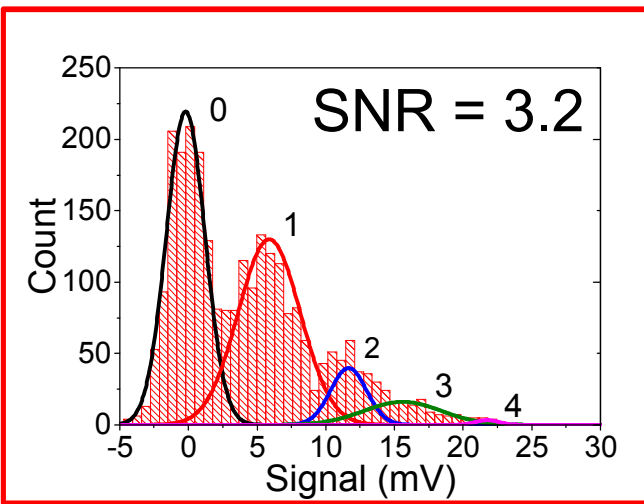


Dominated by Poisson statistics at low ion current

Single Ion Detection



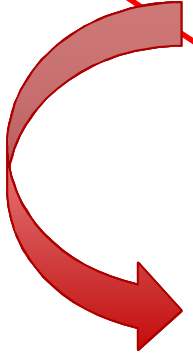
Quantized Detection <0.65> ion



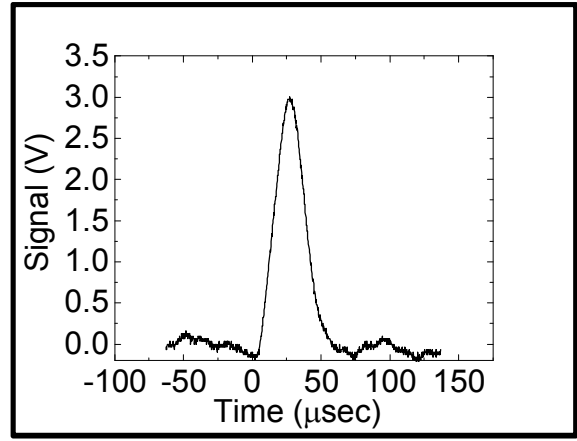
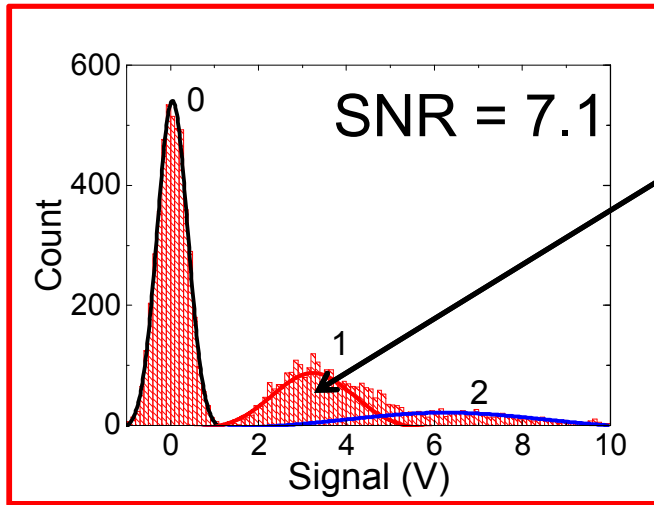
$$SNR = \frac{\mu_{signal}}{\mu_{noise} + \sigma_{noise}}$$

Signal amplitudes match Poisson statistics to 3%

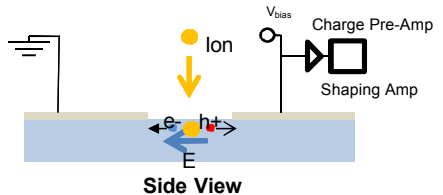
Optimizing gain for single ion detection



Single Ion Counting <0.2> ion

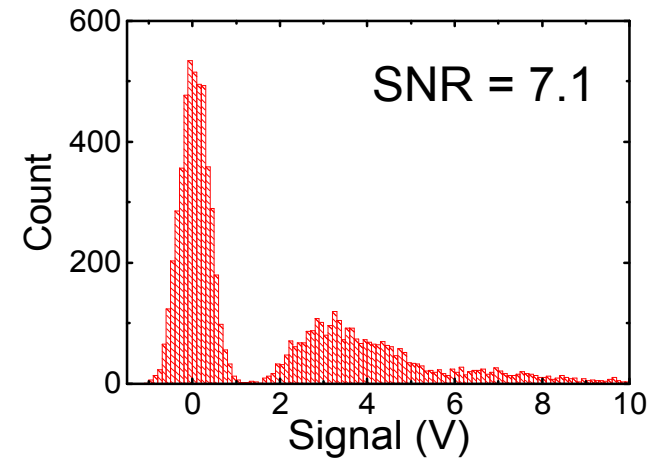


Gate signal for ion beam



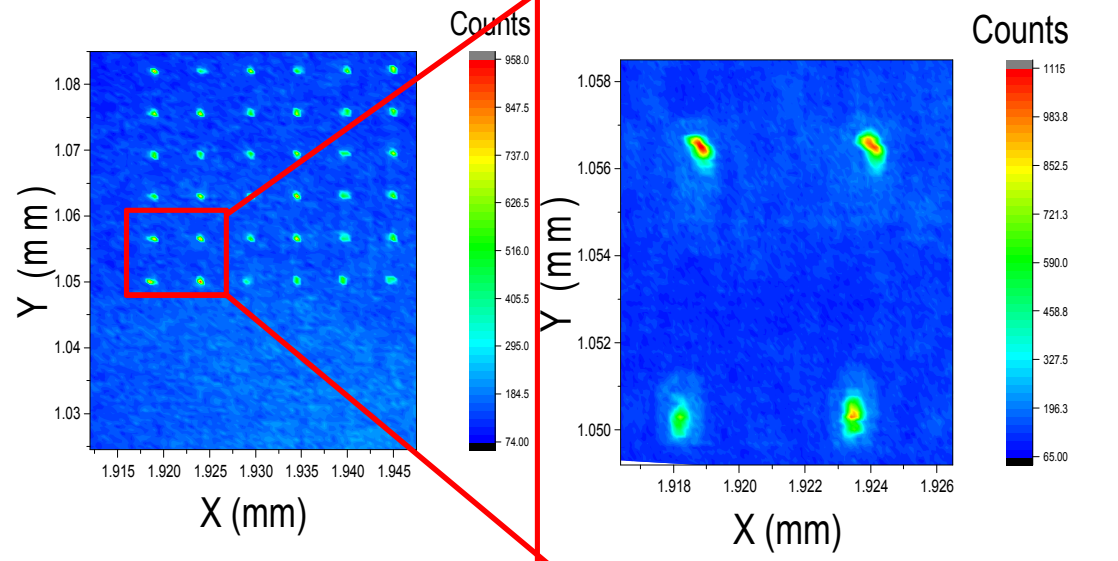
Conclusion/Outlook

- Conclusion:
 - Goal: Counted implantation to minimize Poisson statistics of SiV yield
 - Status: In-situ single ion detection with SNR=7.1



- Follow on work:
 - Measure the yield of a counted implantation.
 - We are in the process of setting up the measurements for yield – PL and g2

738 nm photoluminescence (PL) of timed SiV

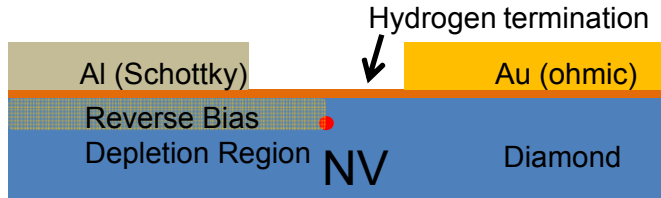


State-of-the-Art Diamond Electronics

Charge state control and electroluminescence have been demonstrated in separate devices

Charge State Control

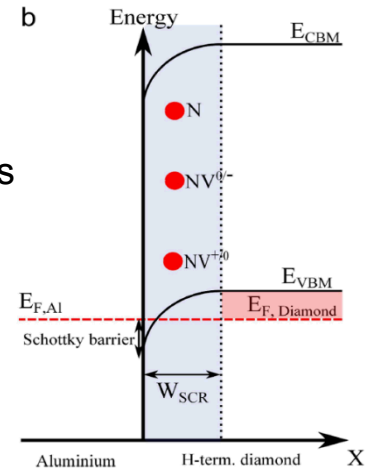
Schottky Diode:
Charge state control via Fermi energy control



Schreyvogel, C. et al., Active charge state control of single NV centers in Diamond by in-plane Al-Schottky junctions, Sci. Rep. 5, 12160 (2015)

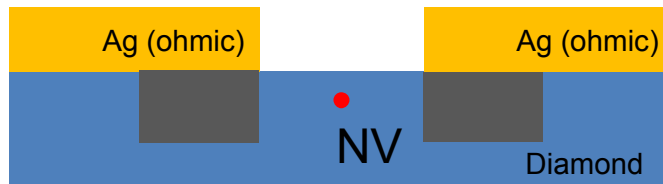
Tuning the occupation of states via reverse bias

Only the specific charge states are coherent emitters (NV^- , SiV^-)
→ Impacts yield

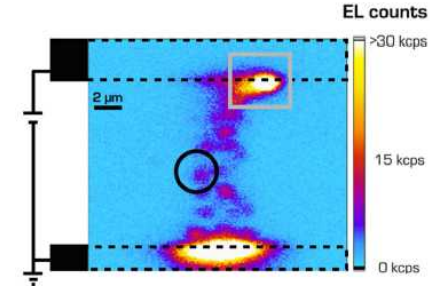
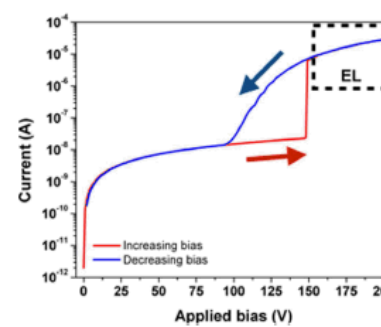


Electroluminescence

Graphitized Electrodes:
Electroluminescence via carrier recombination local to the defect



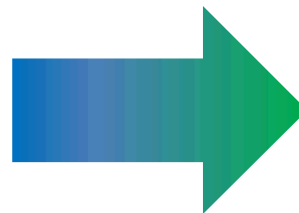
Forneris, J. et al., Electrical stimulation of non-classical photon emission from diamond color centers by means of sub-superficial graphitic electrodes, Sci. Rep. 5, 15901 (2015)



EL → Direct electrical control of emission

Leverage focused ion beam implantation to integrate:

- Charge state control
- Electroluminescence



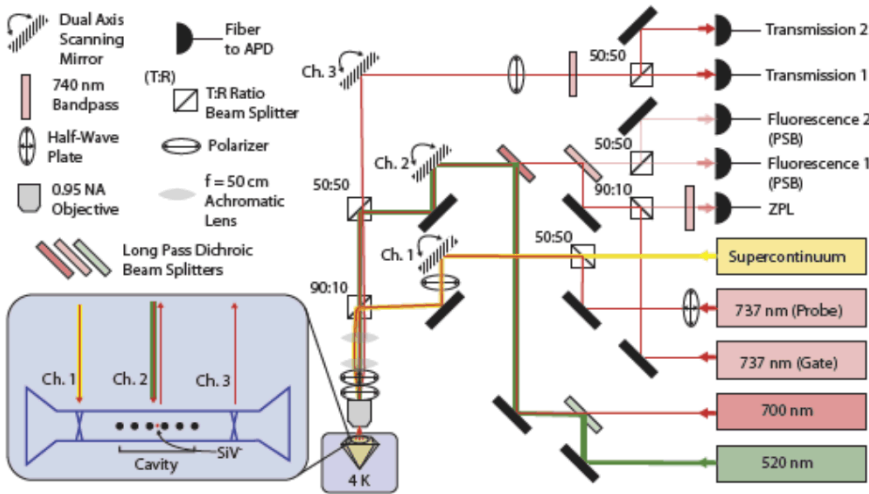
Integrated device to allow for

- Electrical charge state control of color center
- Electrical switching of color center

Goal: Solid-state Distributed Computing

Purpose of this LDRD → Electro-optical control of SiV

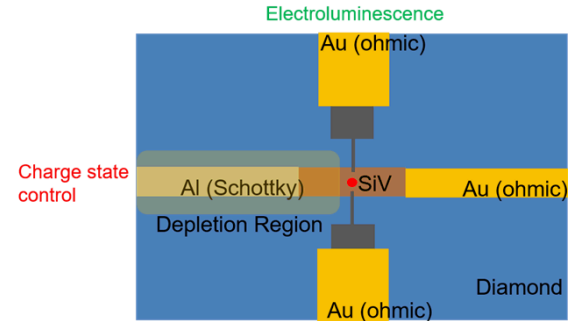
Optical Setup



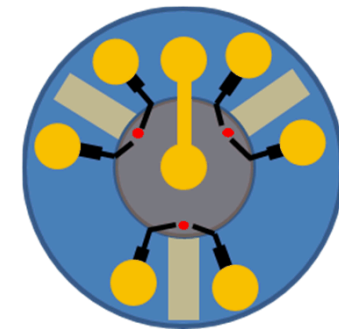
Complex optical setup controls a **single** SiV color center!

- 1.) 520 nm for initialization via photoionization to SiV⁻
- 2.) 700 nm pump for non-resonant excitation
- 3.) 737 nm for cavity transmission

Electro-optical Setup



Initialization: Charge state control
Emission: Electroluminescence



Electro-optical setup scaled to control multiple SiV centers

Take Diamond from a one-off demonstration to wafer scale fabrication

Measurements of the Critical Casimir Effect in Superfluid ^4He Films

John Abraham
Gary Williams
Konstantin Penanen



UCLA

JPL

Jet Propulsion Laboratory
California Institute of Technology

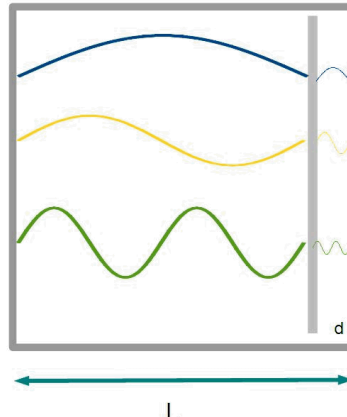
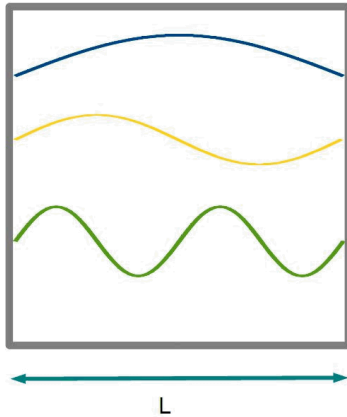
Agenda

- The Casimir Effect
- Superfluid Helium
- The Experiment
- The Results

The Casimir Effect

$$E_{\text{box}} = \sum \hbar \omega_{\text{box}}$$


$$E_{\text{gap}} = \sum \hbar \omega_{\text{gap}}$$



$$\Delta E = -\hbar c \frac{(\pi L)^2}{24 \times 30} \frac{1}{d^3}$$

(Casimir, 1948)

- Universal energy difference from excluding fluctuations(modes)
- Extended to Critical Systems by M. Fisher and P. de Gennes (1978)

Electromagnetic Field  Order Parameter Field
(function of Temperature)

Superfluid ^4He

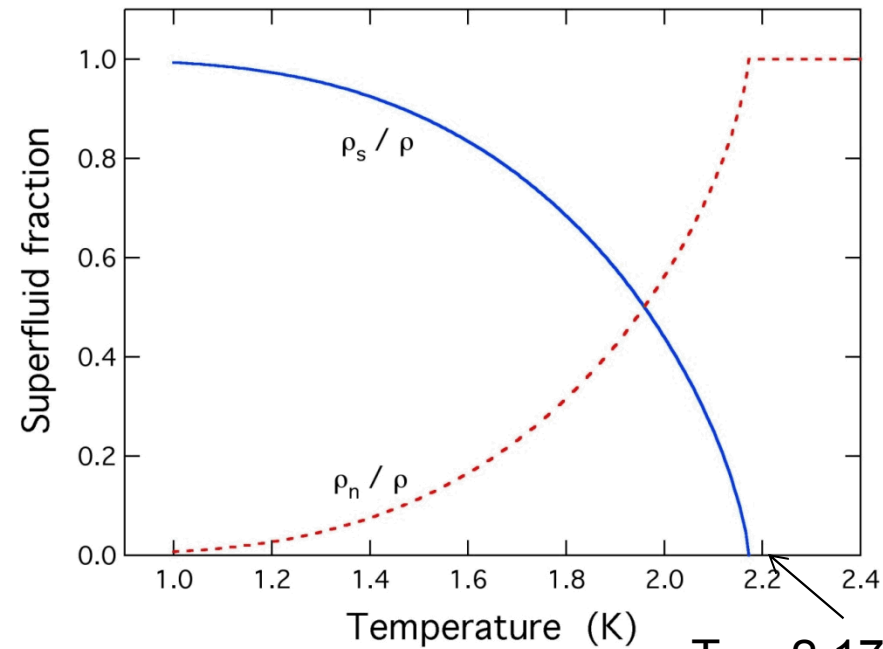
Two Fluid Model (Landau):

$$\rho = \rho_n + \rho_s$$

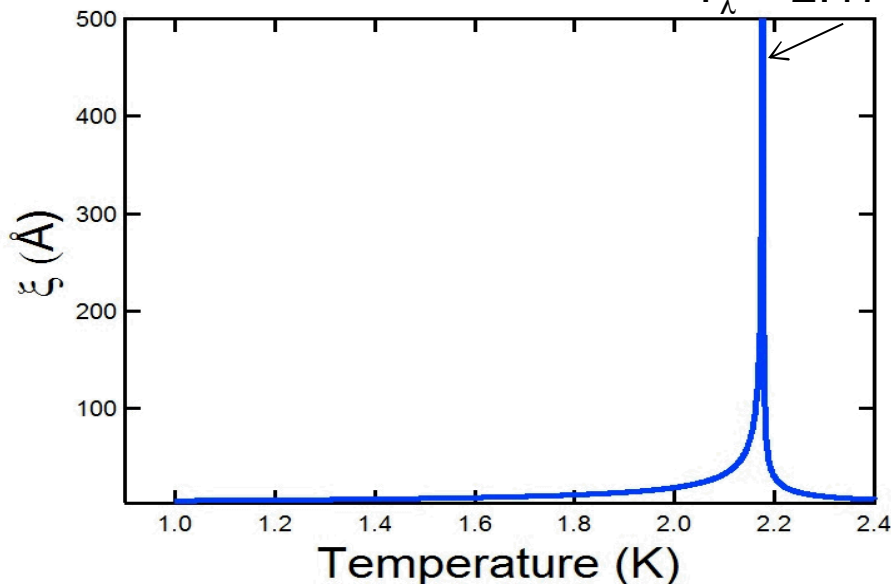
ρ_s has no viscosity

Thermomechanical (TM) Effect:

$$\Delta T \rightarrow \Delta P$$



$$T_\lambda = 2.1768 \text{ K}$$



In terms of the coherence length:

$$\rho_s = \frac{m_{\text{He}} k_B T}{\hbar^2} \xi^{-1}$$

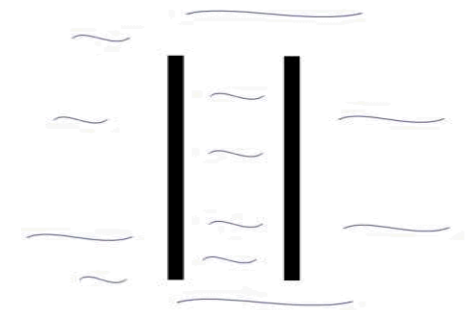
$$\xi = \xi_{\pm} |t|^{-\nu} \quad t = T/T_\lambda - 1 \quad \nu = 2/3$$

What Happens When $d \sim \xi$?

- 2-D Superfluid Transition at T_{KT}

Discontinuous drop of ρ_s in the film at T_{KT}

T_{KT} scales with film thickness, $T_{KT} < T_\lambda$



- The Critical Casimir Effect

Reduction of modes in the Film



ΔE between Film and Bulk



Film thinning

Goal: Measure where the T_C of the film is relative to the Critical Casimir Effect

Superfluid ^4He Films

$$mgh = U_{vdW} = \frac{\alpha_{vdW}}{d^3} \quad (\text{far from } T_\lambda)$$

- Normal fluid is pinned down by viscosity for a film height less than $54 \mu\text{m}$ at audio frequencies

- Can use surface waves to measure ρ_s

$$\delta = \sqrt{\frac{2\eta}{\omega\rho_n}}$$

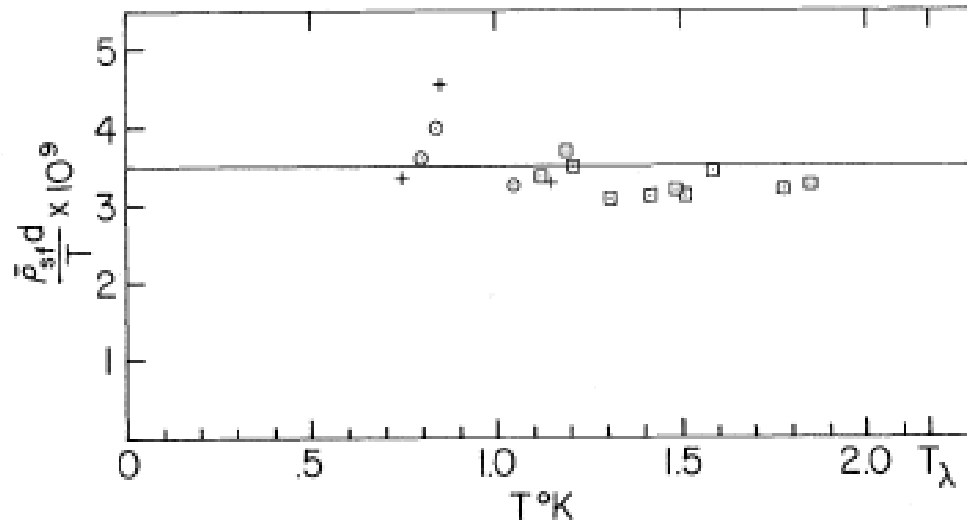
$$C_3^2 \propto \frac{\langle \rho_s \rangle}{\rho} \frac{3\alpha_{vdW}}{d^3}$$

h

h (cm)	10	1	.1
d (Å)	145	280	525

Previous KT Measurements

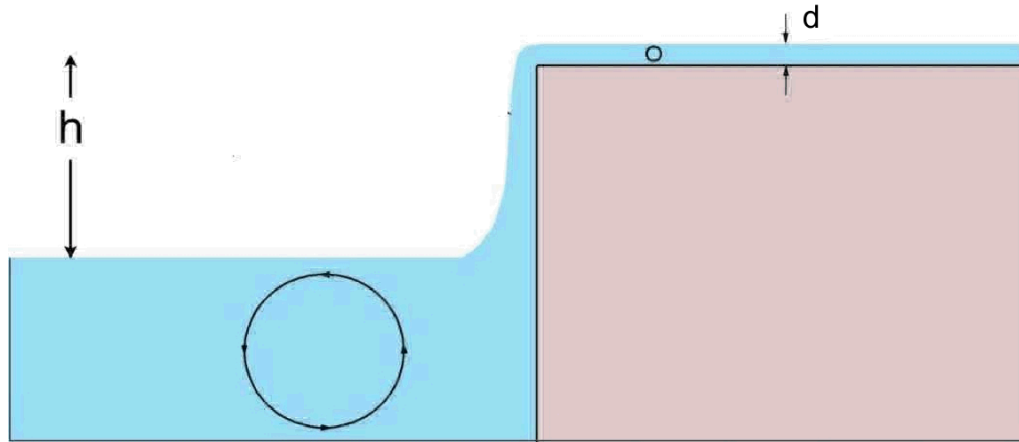
I. Rudnick, Phys. Rev. Lett. (40) 1454, (1978)



I. Rudnick analyzed 3rd sound data at the superfluid onset for different film thickness and validated the ratio of the aerial superfluid density to the transition temperature corresponds to a universal value.

$$\frac{\sigma_s^0}{T_{KT}} = \frac{2}{\pi} \left(\frac{m_{He}}{\hbar} \right)^2 k_B \quad \frac{d}{\xi_{KT}} = 1.59(5)$$

Critical Casimir Effect in ^4He films



- Film thickness determined by:

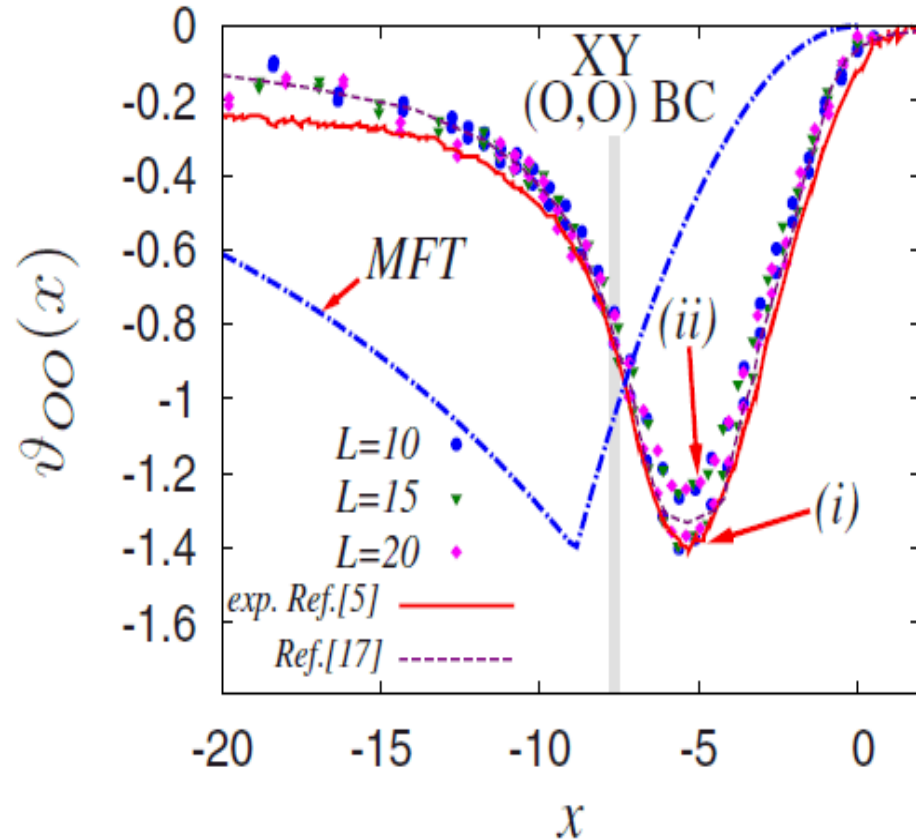
$$\left. \begin{array}{l} \mu(h) = \mu(0) + mgh + \frac{\alpha}{d^3} + E_C \\ \text{Eq. Cond. } \mu(h) = \mu(0) \end{array} \right\} \Rightarrow mgh = \frac{\alpha}{d^3} + E_C$$

- E_C is a finite size universal critical effect which is appreciable only near T_λ , in ^4He this leads to a film thinning

$$d \rightarrow d - \Delta d_{\text{Casimir}}$$

Critical Casimir Effect in ^4He films

O. Vasiljev et. al., Phys. Rev. E **79**, 041142 (2009)



$$x = t \left(\frac{d}{\xi_-} \right)^{1/\nu}$$

■ Casimir Force:

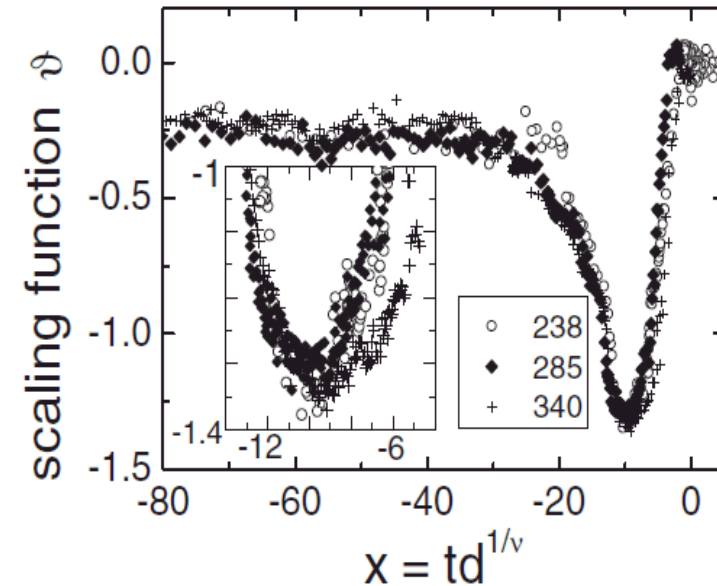
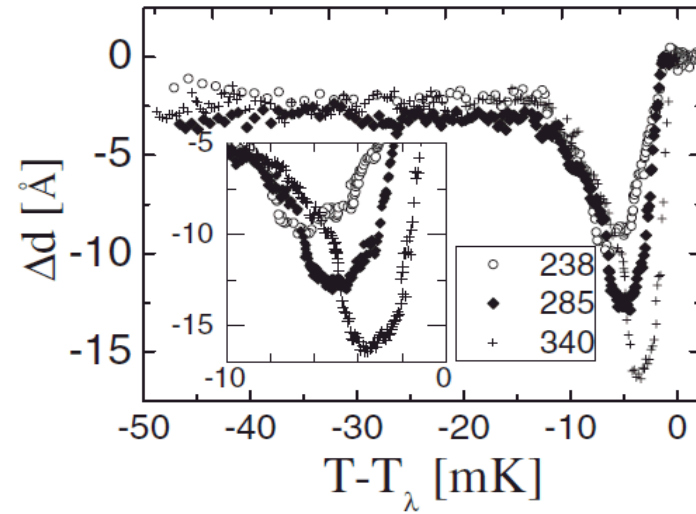
$$E_C = -V \frac{\partial \delta F}{\partial L} = V \frac{k_B T \vartheta}{L^3}$$

- ϑ is a function of L/ξ and depends on the boundary conditions
- Calculations have been made using perturbative ε -expansion, vortex loop renormalization, Monte Carlo, and Mean Field techniques

Critical Casimir Measurements

- First observed by Dionne and Hallock on Ag Substrate (1989)
- Higher resolution measurements (capacitance technique) by Garcia and Chan (1999) on polished Cu
- Further measurements (capacitance technique) by Ganshin et. al. (2006) on Silicon

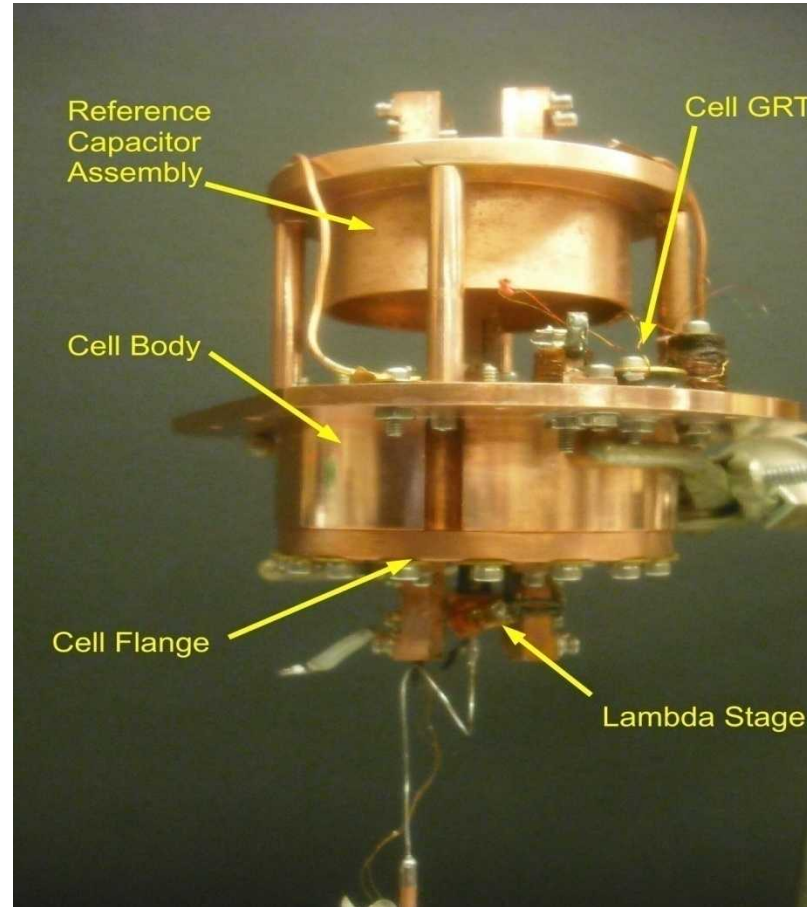
A. Ganshin et. al. PRL 97, 075301(2006)



Experimental Requirements

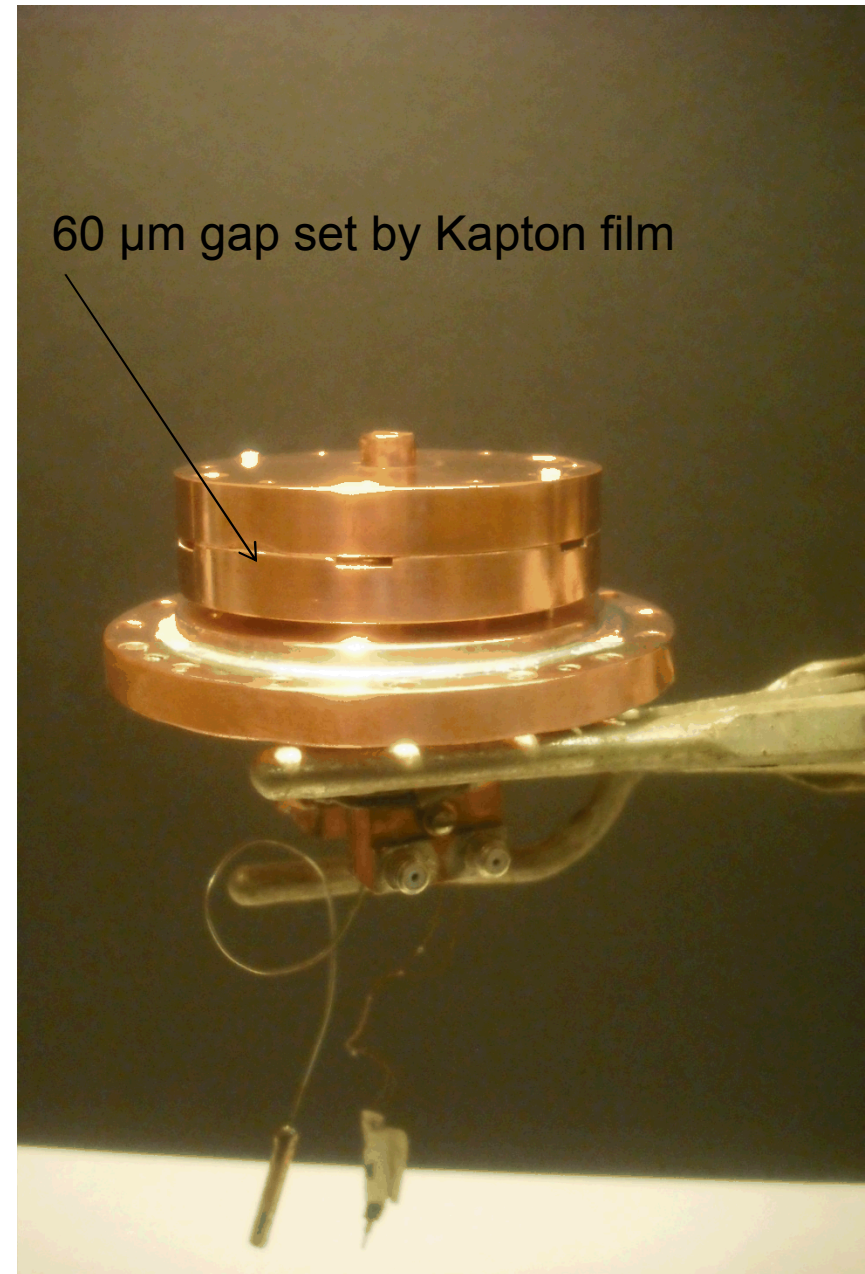
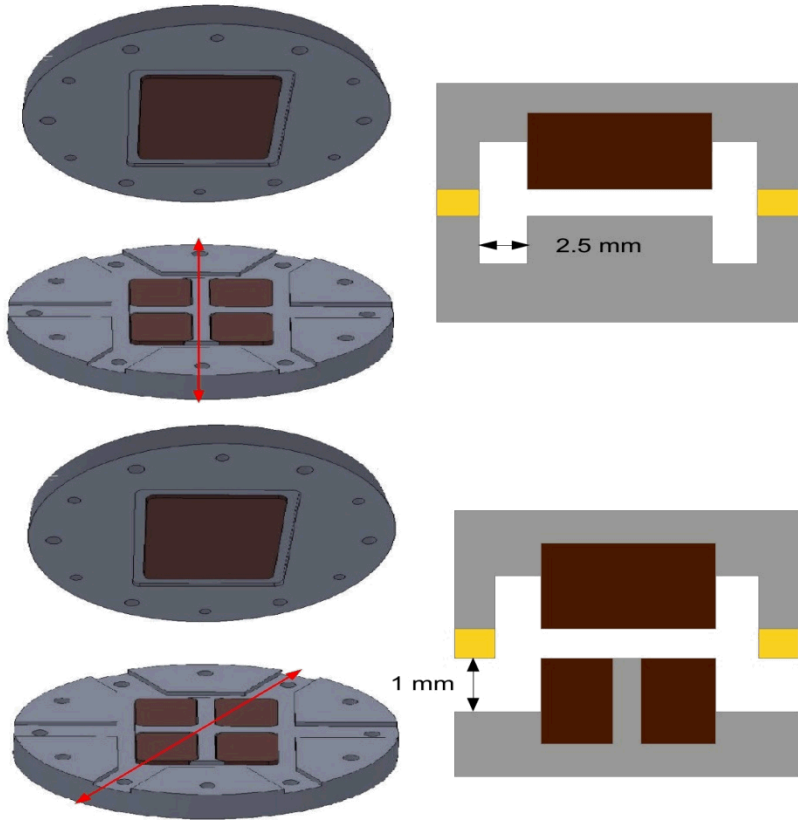
- Thermal Stability: Exploring phenomena in the vicinity of the Lambda transition, $1 \mu\text{K} \rightarrow 1 \text{ \AA}$ from TM Effect, diverging specific heat - λ point.
- Long bath hold times: Transfers disturb the film (~ 1 day to stabilize) and slow temperature sweep times (4 – 200 $\mu\text{K/hr}$)
- Mechanical Stability: Measuring thickness changes in 300 \AA liquid film (pot noise, bath boil off)
- Surface Quality: Roughness $< 100 \text{ \AA}$ for 2D film
- Precision Cryogenic Capacitance Measurement: Experiment requires a sensitivity of $10^{-8} \delta C/C$ over long time periods.

UCLA/JPL Casimir Experiment



- Mounted on custom 1.5 K cryostat supported by air springs
- +/-10 μK stability for days near T_λ - PID feedback control

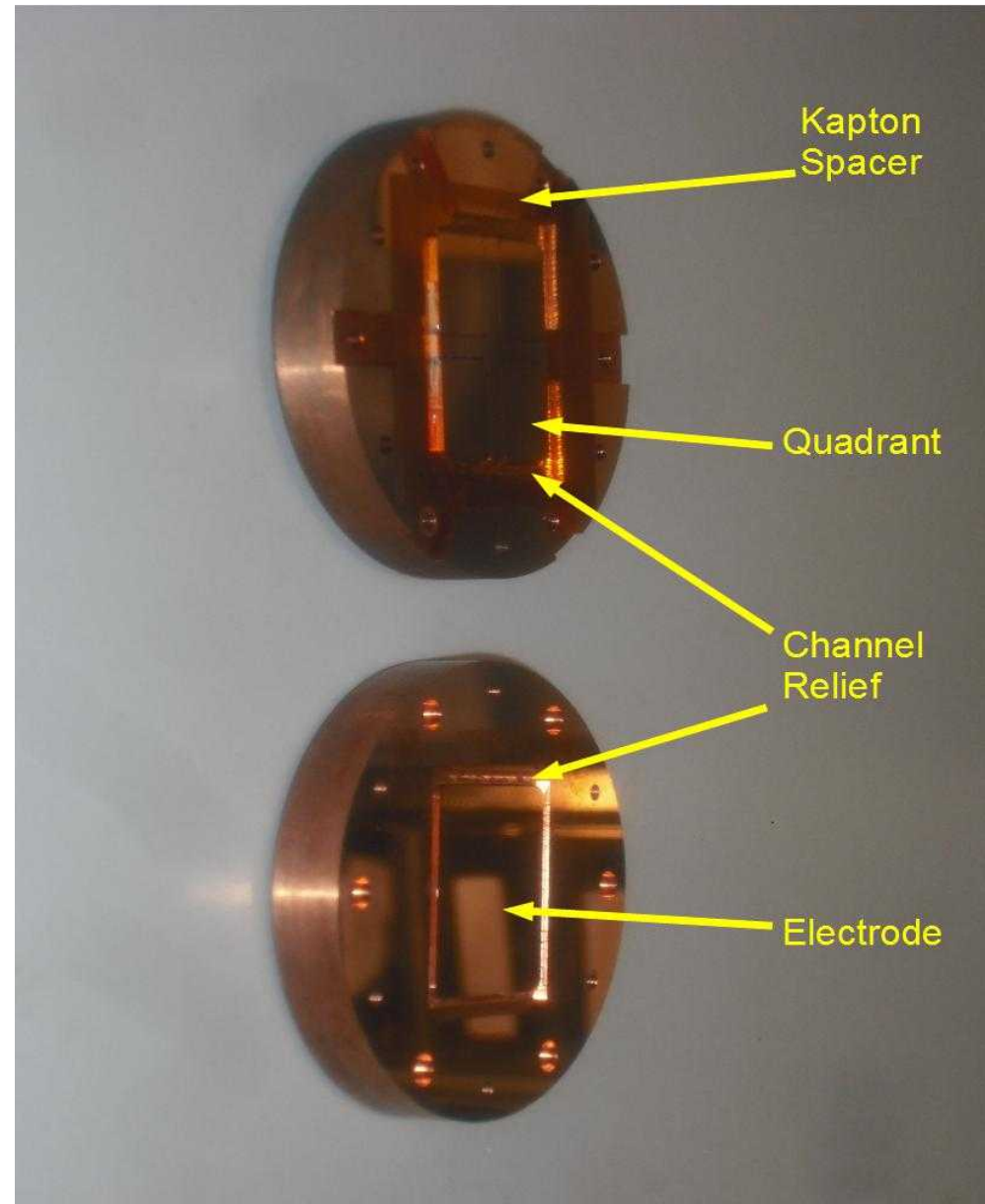
UCLA/JPL Casimir Experiment



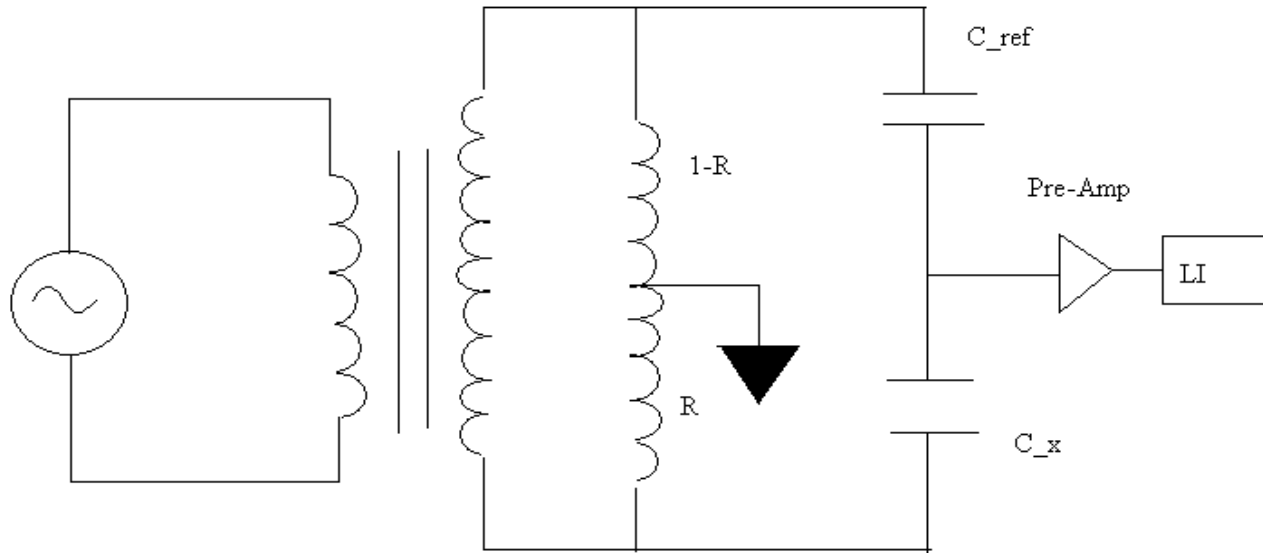
- Measure film thickness via capacitor
- Drive and detect surface waves
- Substrate surface roughness ~ 10 nm

UCLA/JPL Casimir Experiment

- Substrate holders are fabricated and then sent out for diamond turning ($<10 \text{ \AA}$ surface roughness)
- $60 \text{ }\mu\text{m}$ Kapton spacer to set gap
- Connects from the top plate to the electrodes consist of solders, pin contacts, SMA, or BNC connectors
- Channel relief to forestall gap filling for thick films



Film Thickness Measurement



$$C_x = C_{ref} \frac{R}{1-R}$$

$$R = R_{RT} + \frac{\Delta R}{\Delta V} V_{LI}$$

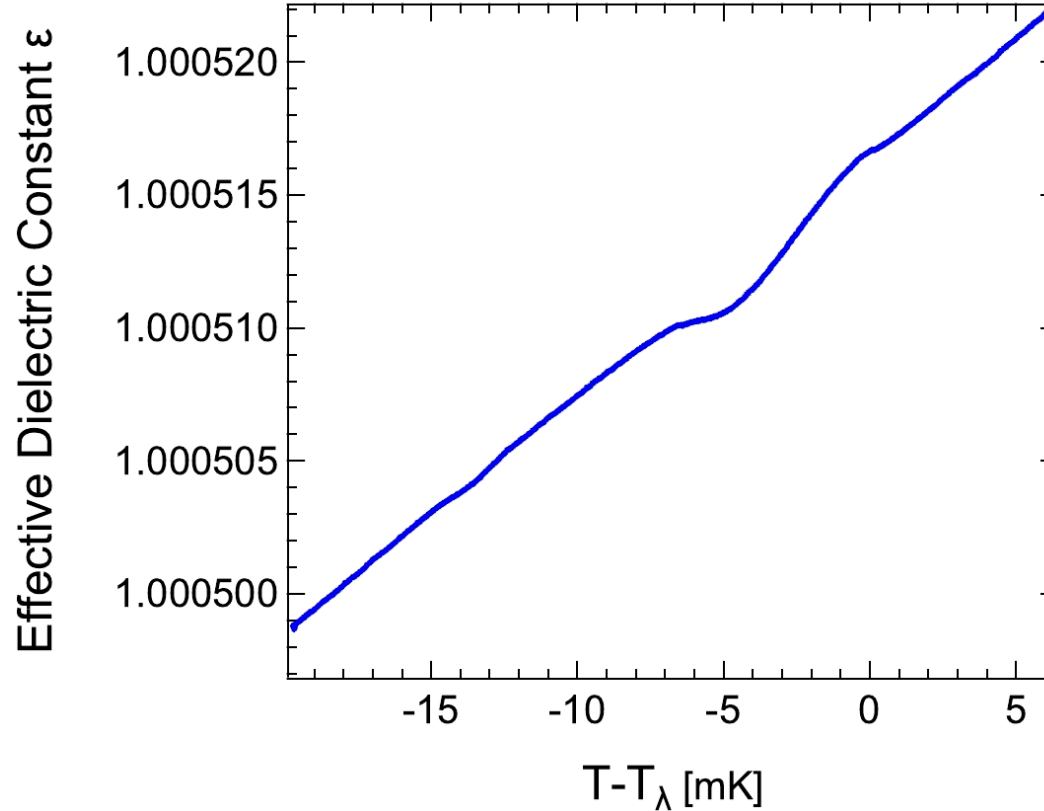
- Dominate noise sources are the thermal stability of the RT and the cell

$$\frac{\partial R}{\partial T} = 10^{-6} K^{-1} \times f^2 \text{ (in KHz)}$$

$$1 \mu\text{K} \rightarrow 1 \text{ \AA} \text{ (TM)}$$

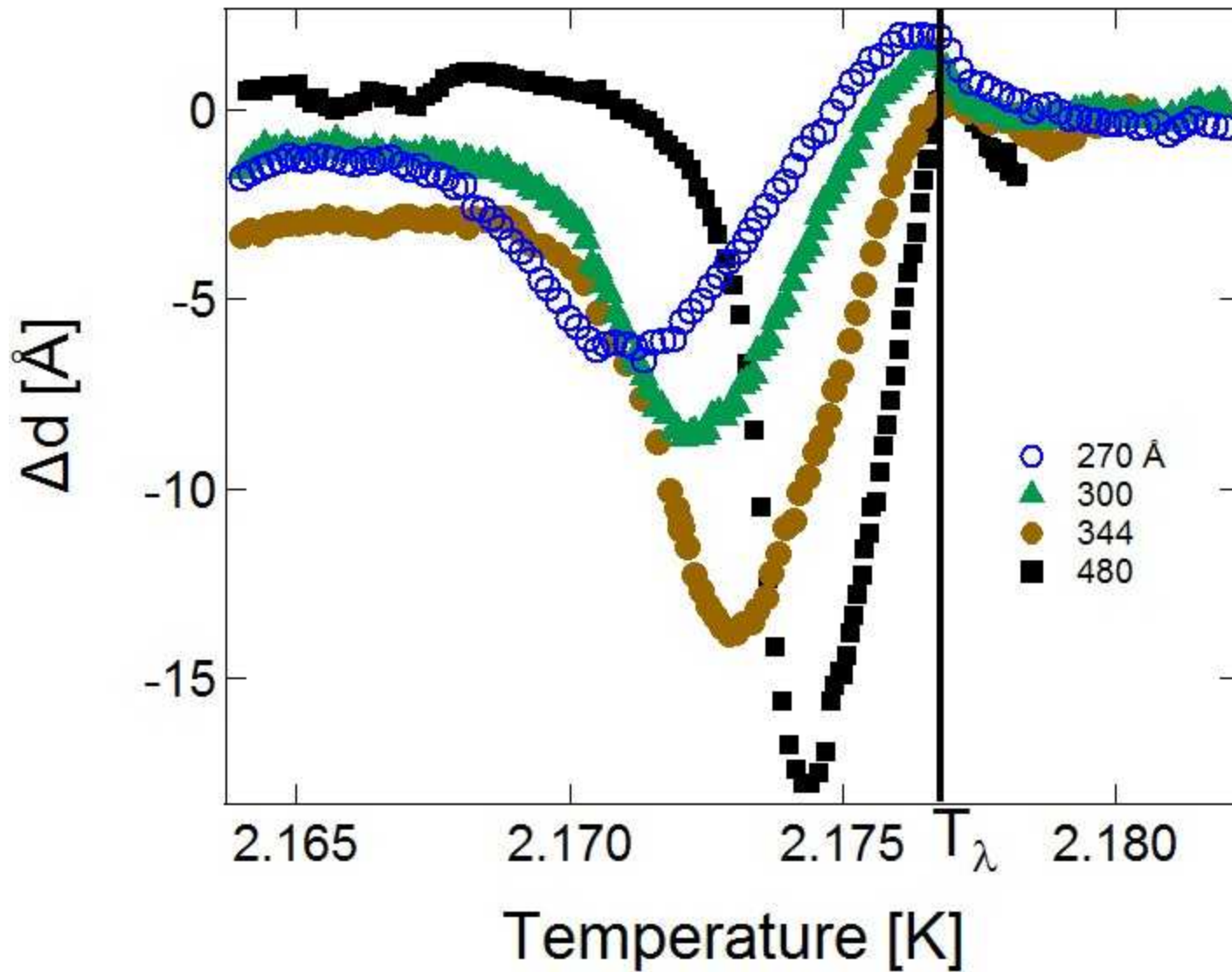
$$\frac{\delta C}{C} = 2.7 \times 10^{-8} \Rightarrow \text{Sub-Angstrom film thickness resolution}$$

Film Thickness Measurement

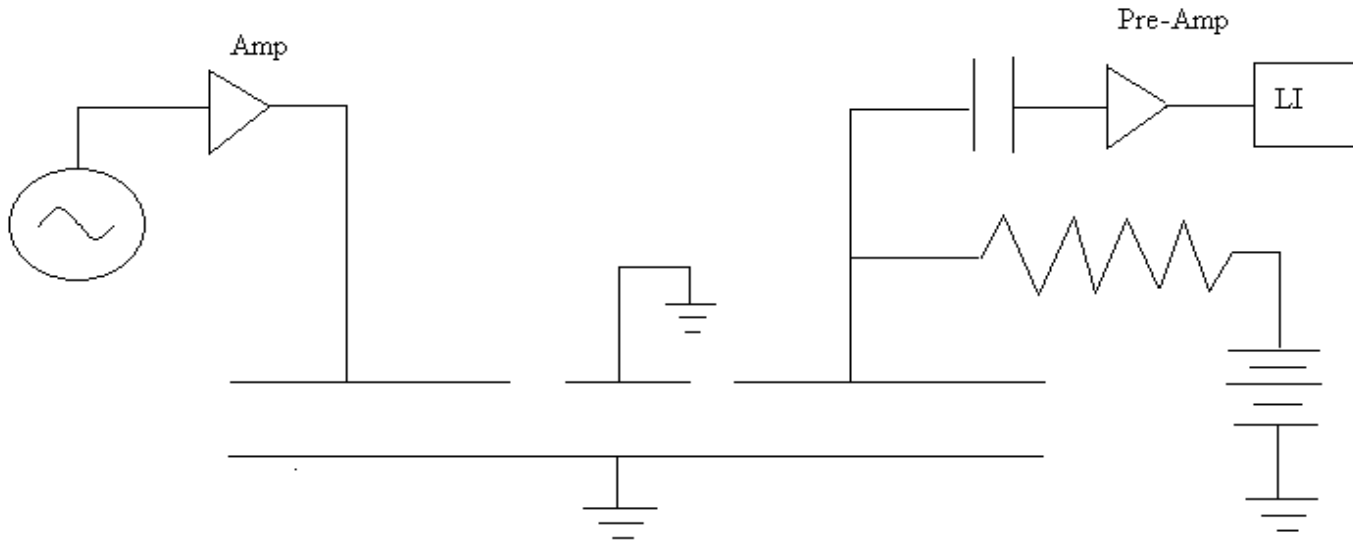


$$d = \frac{G}{2} \left(\frac{1}{\epsilon_{\text{vapor}}} - \frac{1}{\epsilon(T)} \right) / \left(\frac{1}{\epsilon_{\text{vapor}}} - \frac{1}{\epsilon_{\text{film}}} \right)$$

Film Thickness Measurement

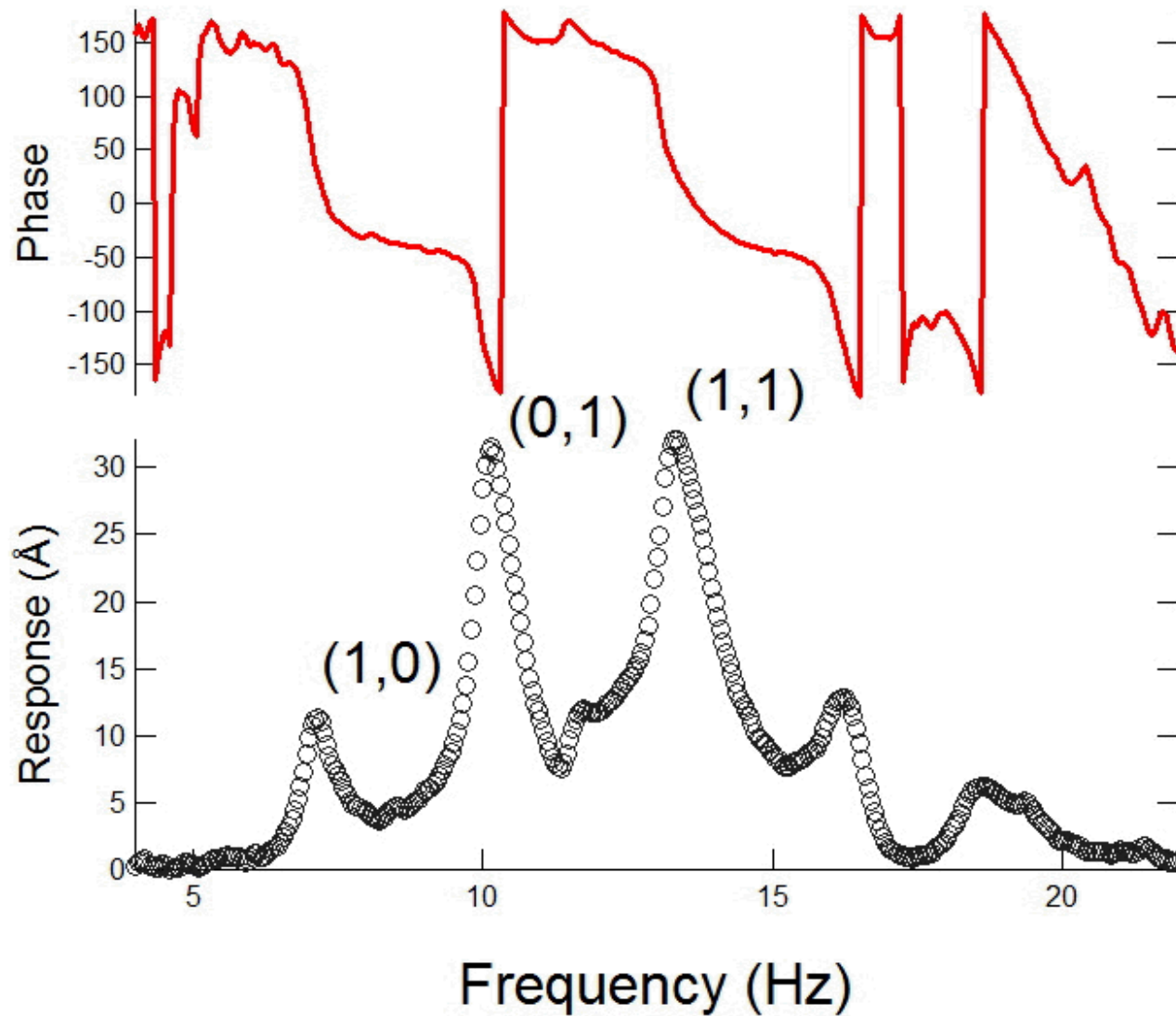


Charge Biased Third Sound



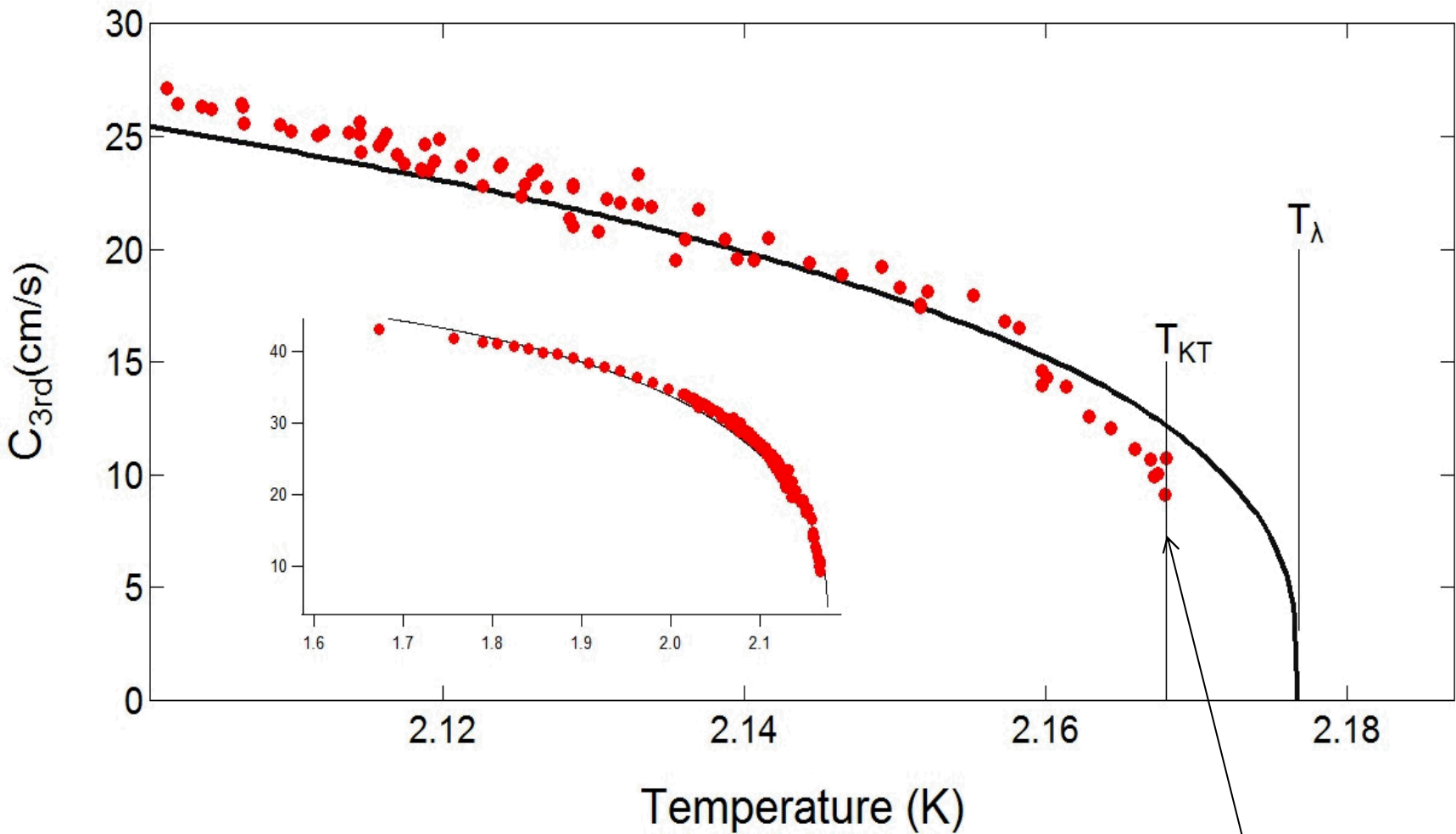
- A 120 V battery is connected to the detection electrode through a large resistance ($1 \text{ G}\Omega$)
- R is set so the RC time is large enough to keep the system in a constant charge regime. The voltage change is proportional to the capacitance change.

Third Sound Measurement



$$C_{3rd} = \frac{\omega}{k}$$

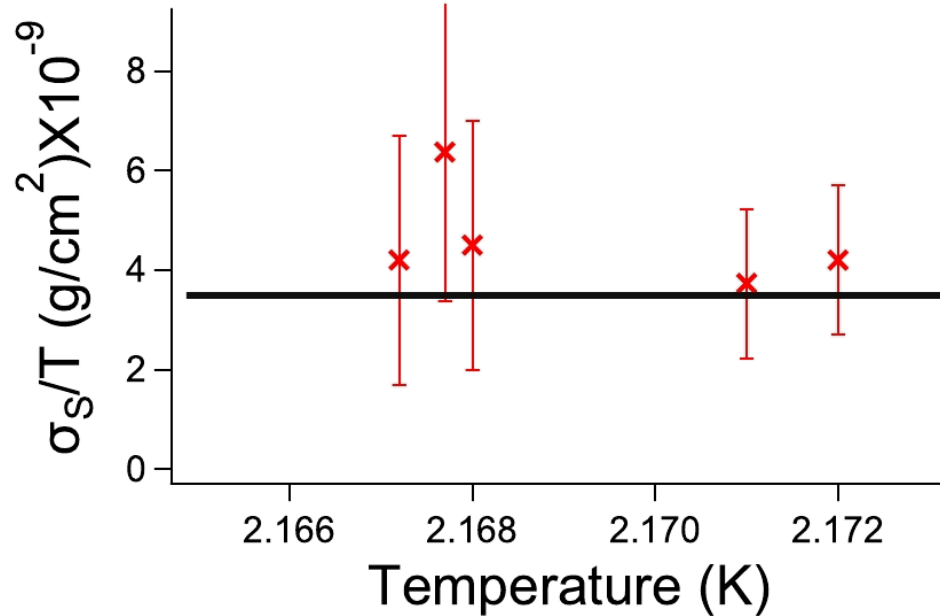
Third Sound Measurement



$$C_3^2 = \frac{\langle \rho_s \rangle}{\rho} \frac{3\alpha_{vdW}}{d^3} \left(1 + \frac{TS}{L} \right)^2$$

Discontinuous drop
to zero at T_{KT}

KT Measurement

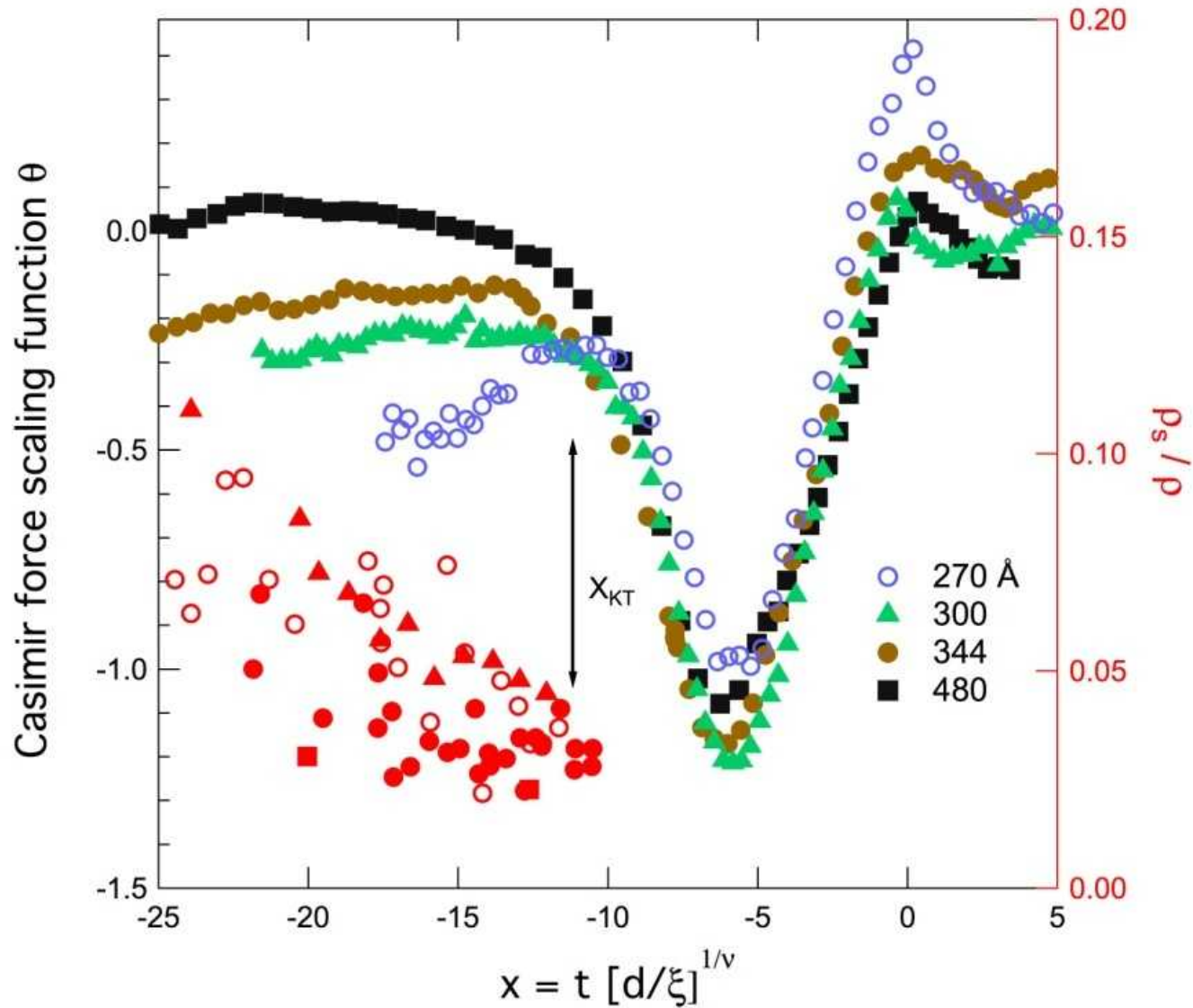


$$X_{KT} = -11.1(1)$$

Result differ from thin film measurements and MC simulations, but agree with thick film measurements of Gasparini (2012)

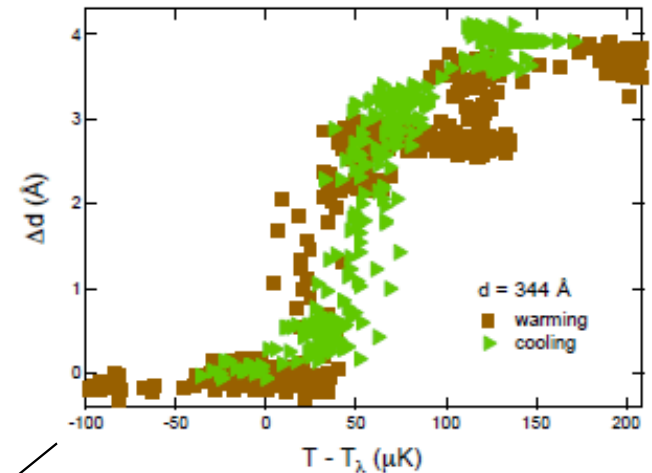
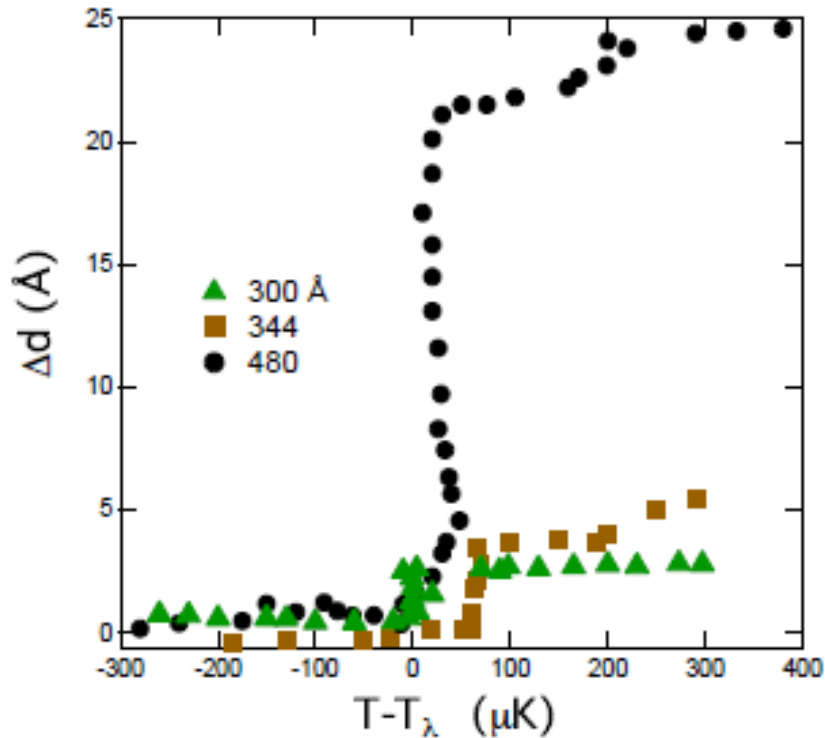
Scaled Casimir force

$400 \mu\text{K} / \text{hr}$



New Casimir effect at T_λ

$4 \mu\text{K} / \text{hr}$



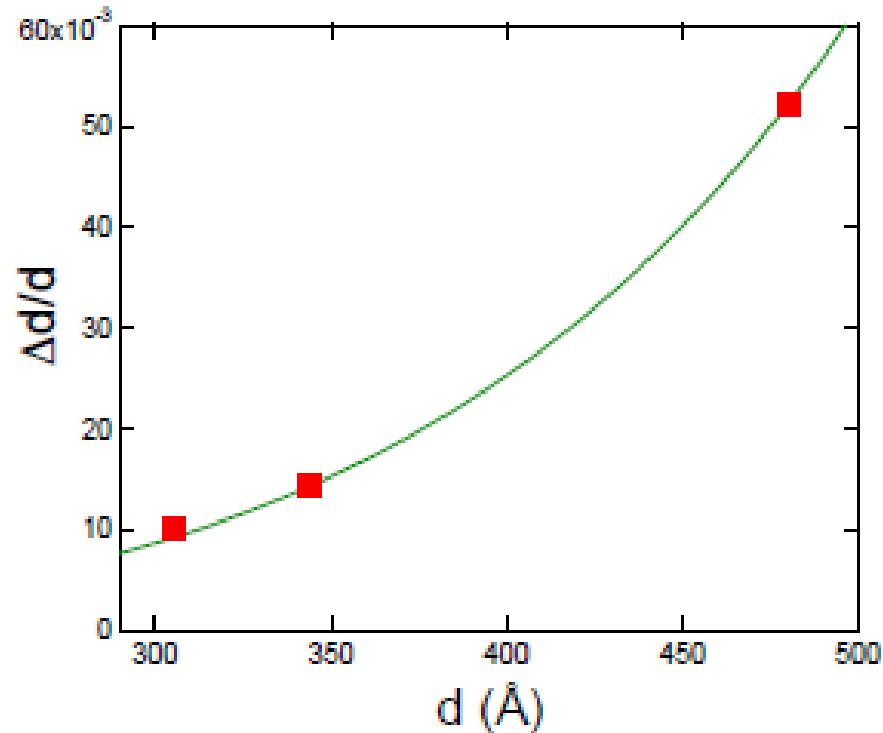
- Sudden jump in equilibrium film thickness at T_λ
- Only observable at very slow temperature sweep rate

Hypothesis: Onset of second sound (thermal waves) in the bulk, but not in the film

What we are not seeing at T_λ

- Thermomechanical effect
 - Effect would not be more pronounced for a slower sweep rate
- Gap filling
 - Same magnitude step observable on other quadrants

New Casimir effect at T_λ



$$\frac{\Delta d}{d} = \frac{\Delta FE}{U_{VdW}} \propto d^3 \quad \Delta FE \cong 3.5 \frac{\text{erg}}{\text{cc}} \rightarrow 1 \mu\text{K} / \text{atom}$$

To our knowledge, this would be the first measurement or estimate of the energy for second sound onset at the transition.

Time constants at T_λ

- Diffusion through the vapor

- Using the Einstein relation for mobility

$$\mu = \frac{D}{kT}$$

- $\tau \sim 10^6$ seconds

- Thermal time constant

- Diverging specific heat and thermal conductivity at T_λ

- $\tau = C/\lambda \sim 10^4$ seconds

- Thermomechanical effect

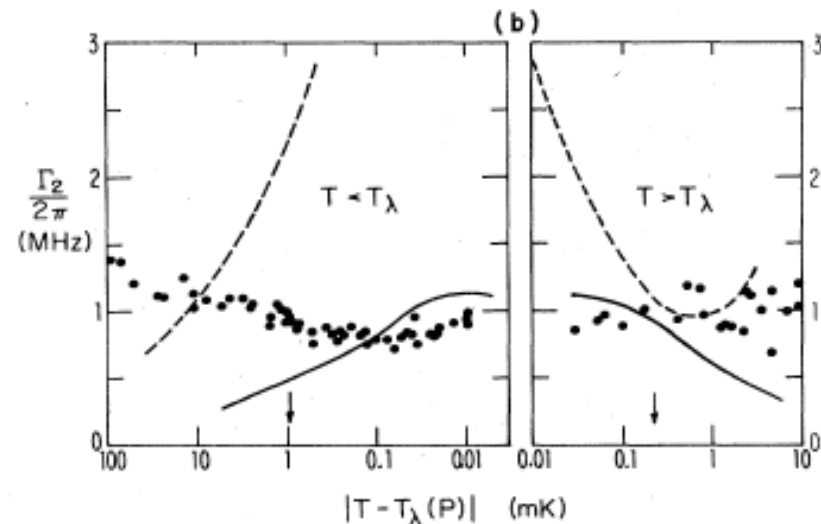
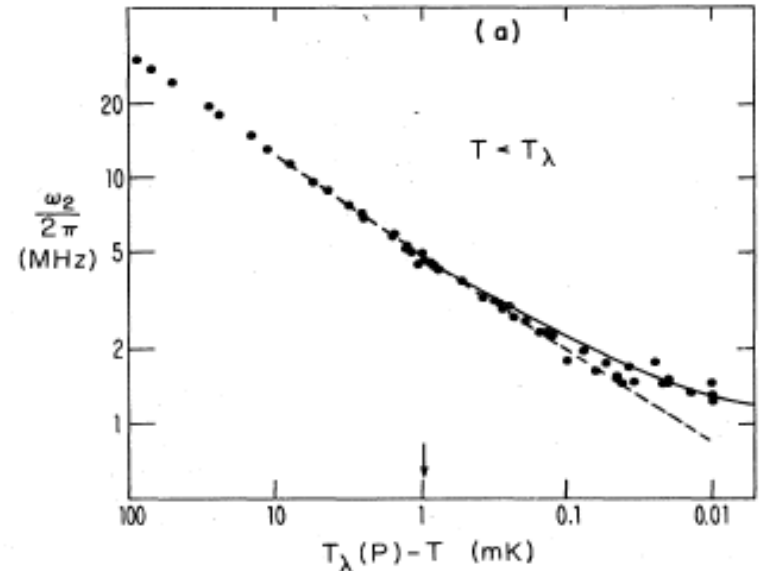
- Film thickness is perturbed by thermal gradients

- $1 \mu\text{K} \rightarrow 1 \text{ \AA}$

2nd Sound in the Critical Regime

Tarvin, Vidal, and Greytak Phys. Rev. B, (15) 4193 (1977)
Hohenberg and Halperin., Rev. Mod. Phys. (49) 435, (1977)

- Extrapolation of hydrodynamic results not valid in critical region where $\xi q > 1$ based on light scattering experiments of Tarvin et. al. (1977)
- ΔFE at T_λ provides a new result for developing the understanding of dynamic critical phenomena



Debye Model at T_λ

$$\Delta FE = \frac{k_b T}{2\pi^2 c_2^3} \int_0^{\omega_D} \omega^2 \ln\left(\frac{\hbar\omega}{k_b T}\right) d\omega$$

$$= -\frac{k_b T}{2\pi^2} \left(\frac{\omega_D}{c_2}\right)^3 \left[\frac{1}{9} - \frac{1}{3} \ln\left(\frac{\hbar\omega_D}{k_b T}\right) \right]$$

$$\frac{\hbar\omega_D}{k_b T} \ll 1$$

- Using the Debye model, our result, and the c_2 results:

The cutoff $\omega_D = 6$ MHz

Future Directions

- SQUID based HRT Thermometry
 - Sub-nK temperature resolution
- Actuator height control
 - Change film height without changing bulk sample (bellows?)
- Alternate techniques
 - MEMS resonator
 - Vapor pressure measurement

Summary

- Film undergoes 2-D transition at the start of dip in film thickness
- Critical Casimir effect agrees with scaling theory
- Observation of a new abrupt change in film thickness at T_λ

Hypothesis: Second sound (thermal waves) onset in the bulk, but restricted in the film → **non-universal Casimir force detection of 2nd sound onset**

- Not something you will find via MC simulations

Figure 2: Detector Characterization I

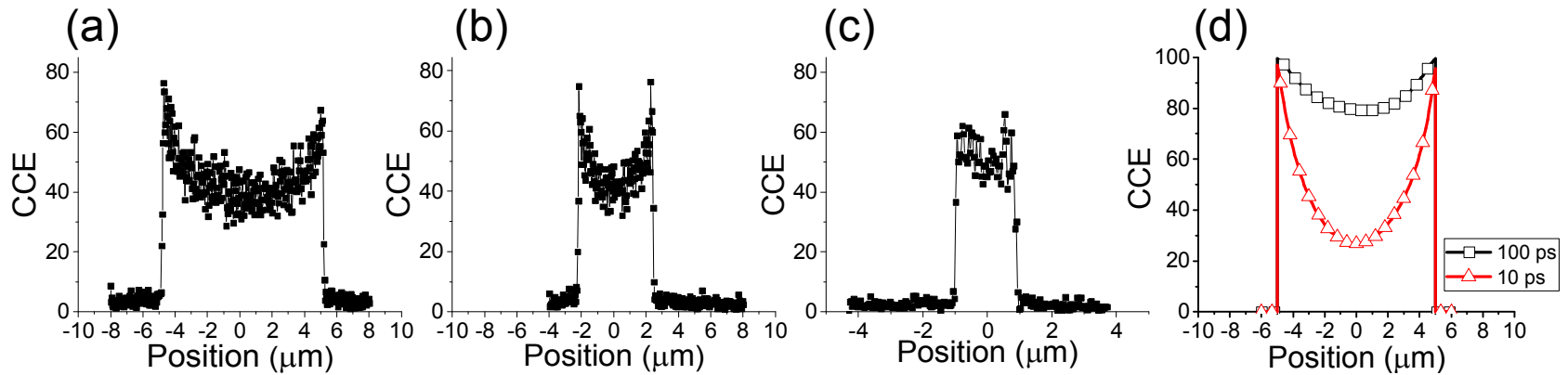
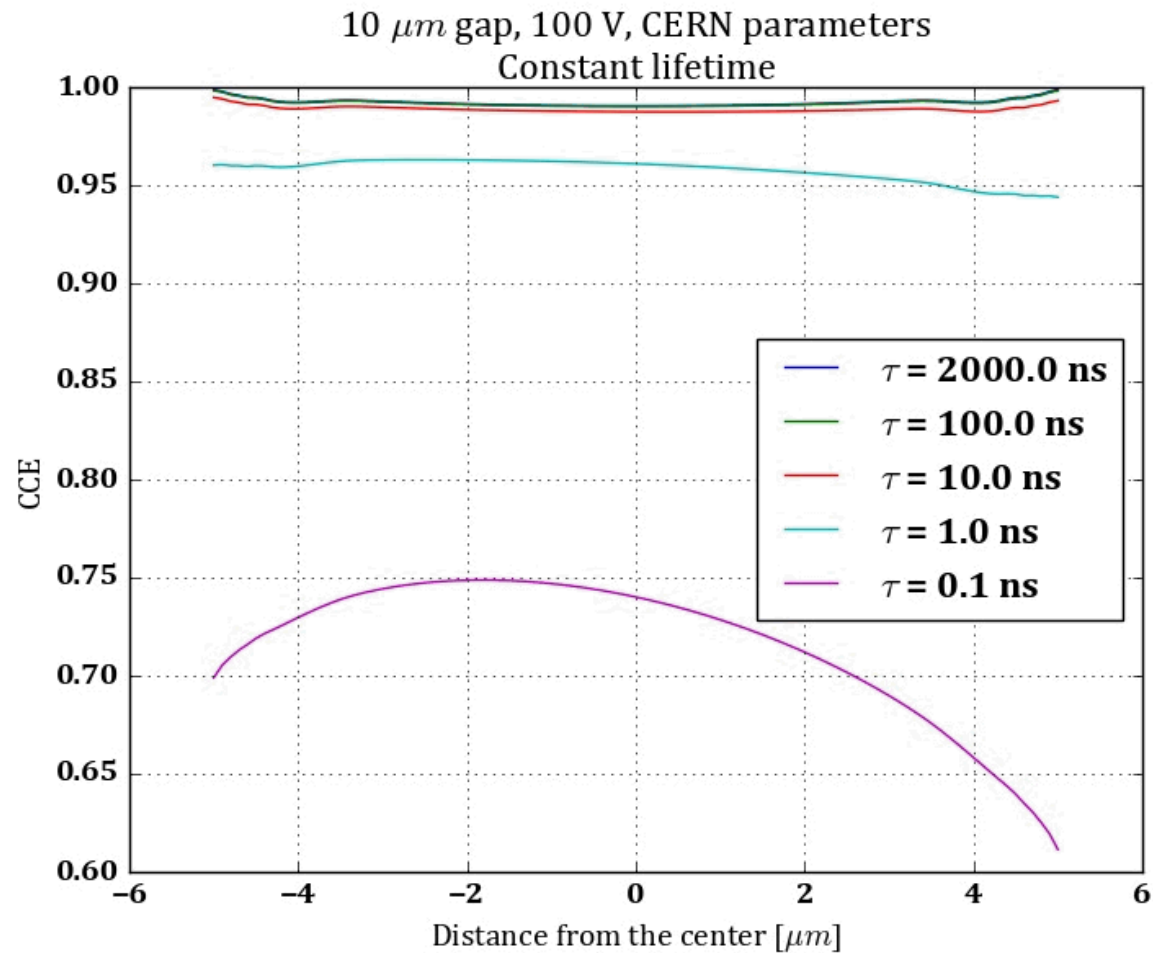


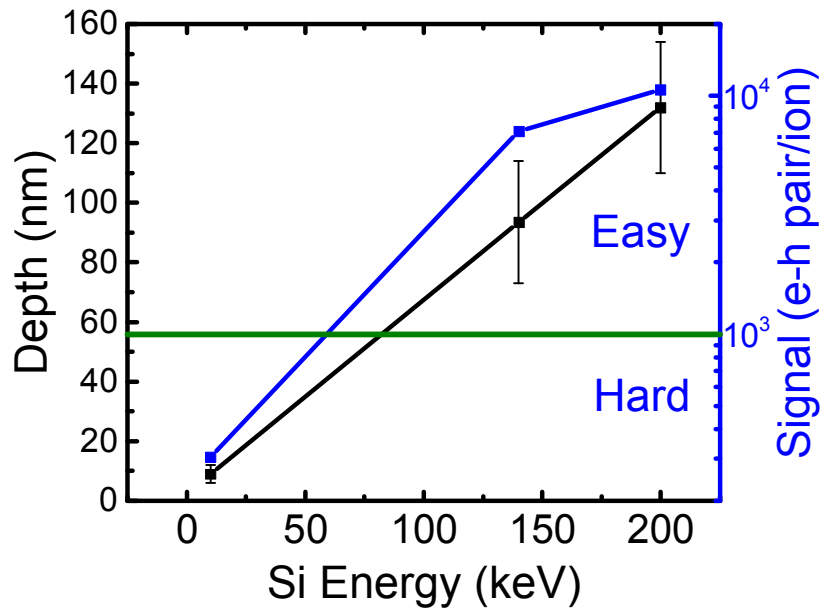
FIG. 2. (color online) IBIC line scans taken across devices with (a) 10 μm , (b) 5 μm and (c) 2 μm gaps using 100 ions per pulse with 10 V/ μm of scaled bias (the bias divided by the gap size). (d) CCE simulation with reduced carrier lifetimes (10 and 100 ps) in the shallow implantation region.

Constant lifetime

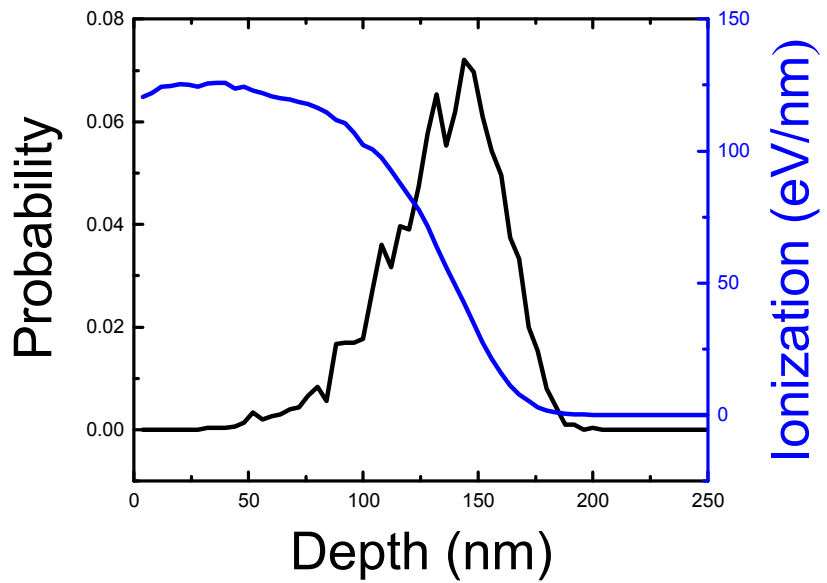


Monte Carlo Simulation (SRIM)

Si implantation

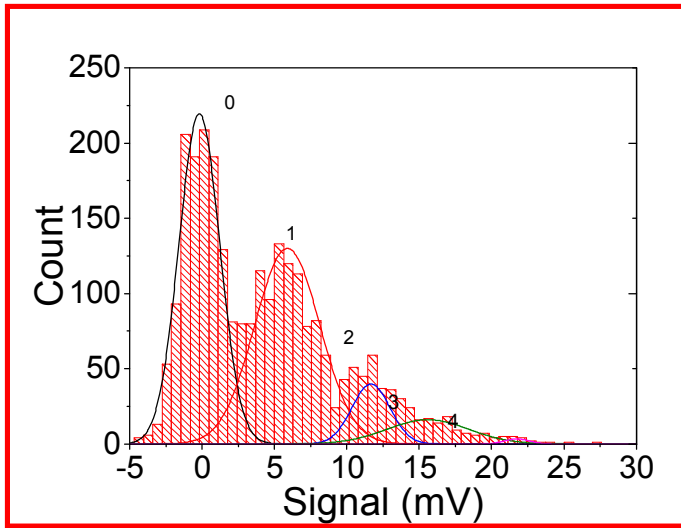


200 keV Si implantation

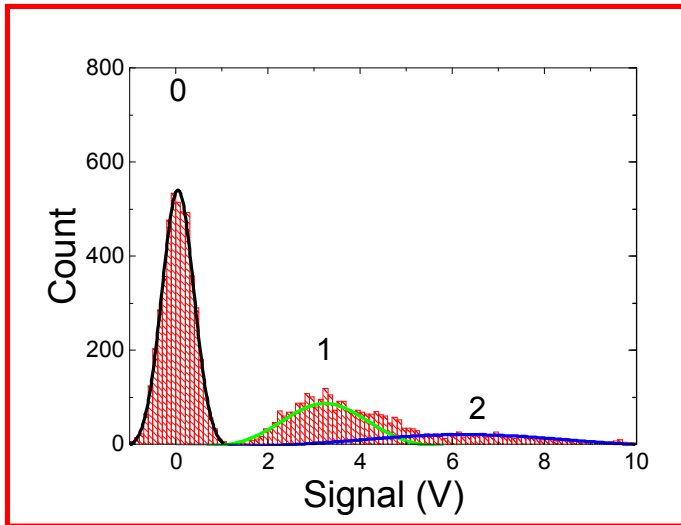


- 200 keV Si into diamond
 - 132+/-22 nm depth
 - 10⁴ e/h pairs deposited in 75 nm depth

Poisson Statistics of Detection



Number of ions	Measured probability	Poisson distribution for $\langle 0.65 \rangle$ ions
0	0.537	0.5221
1	0.319	0.3393
2	0.098	0.1103
3	0.039	0.0239
4	0.007	0.0039
>4		0.0005
Total	1	1

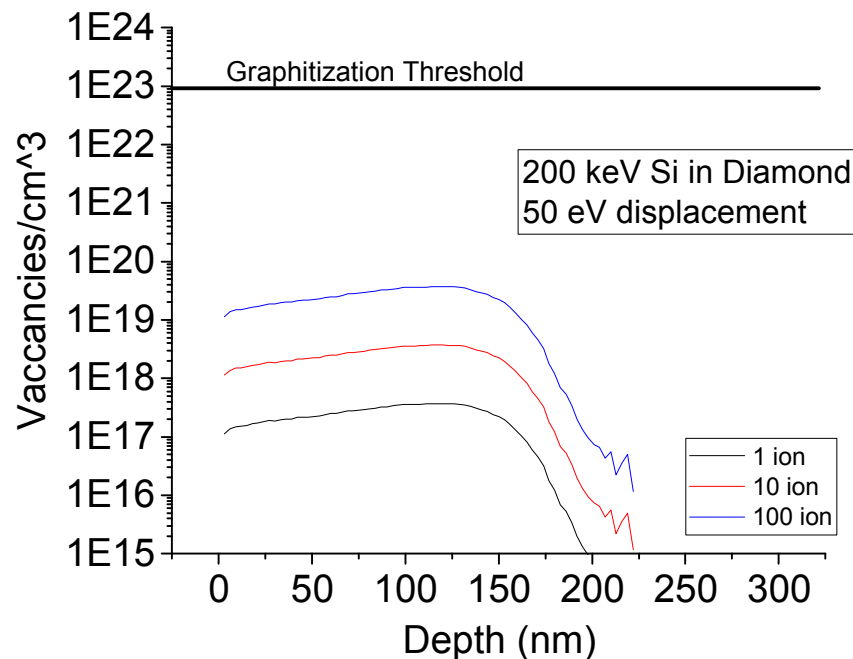


Number of ions	Measured probability	Poisson distribution for $\langle 0.2 \rangle$ ions
0	0.816	0.819
1	0.141	0.164
2	0.043	0.016
>2		.001
Total	1	1

Remaining Detector Questions

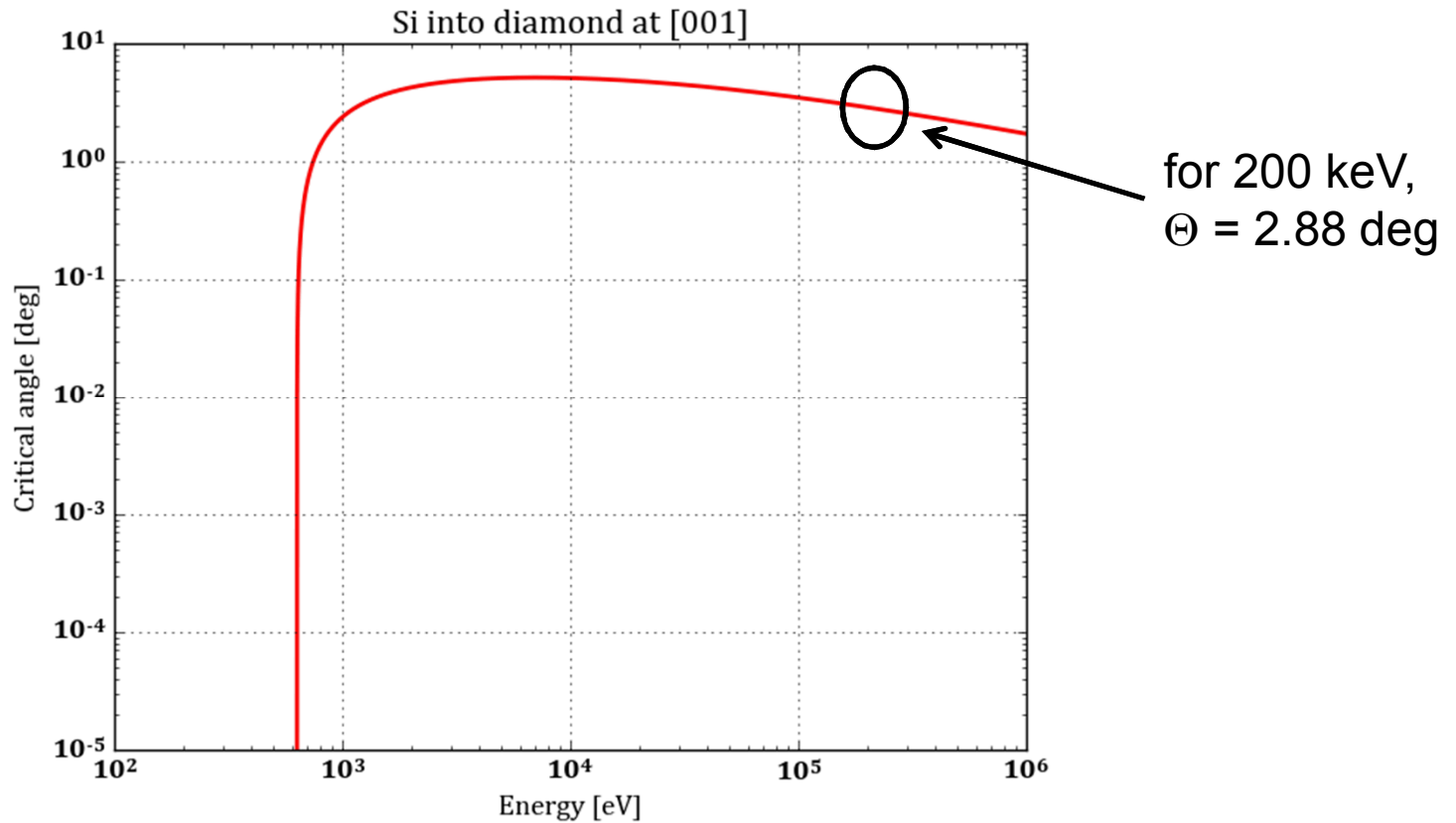
- Linearity of response
 - CCE seems to drop off above 10 ions/pulse...

SRIM simulation of
damage for implantation



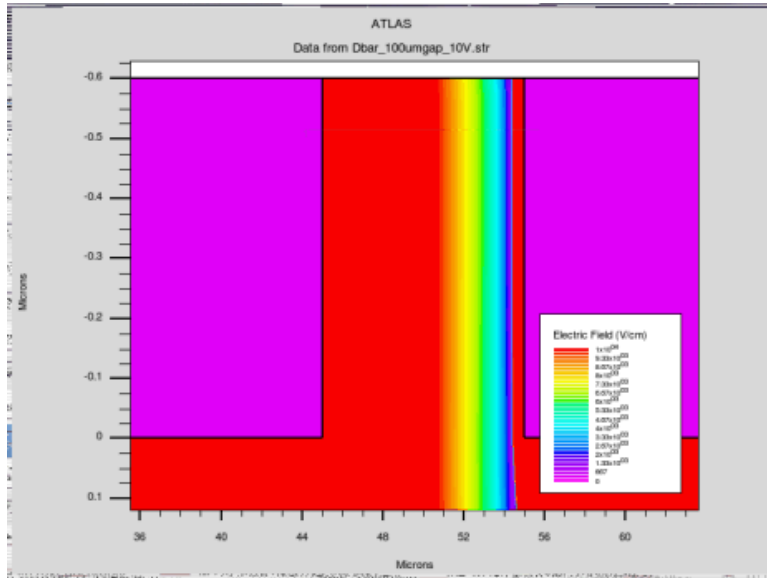
Need to generate a plot of CCE versus
Dose for existing data.

Channeling?



MARLO Simulation by George Vizkelethy

How to improve



Paulos stuff with corrugated thing

